# Group action Markov chain Monte Carlo for accelerated sampling of energy landscapes with discrete symmetries and energy barriers

## Matthew Grasinger

Materials and Manufacturing Directorate, Air Force Research Laboratory, WPAFB, Dayton, OH 45432, USA

#### Abstract

Monte Carlo sampling of the canonical distribution presents a formidable challenge when the potential energy landscape is characterized by a large number of local minima separated by high barriers. The principal observation of this work is that the multiple local minima and energy barriers in a landscape can often occur as a result of discrete symmetries in the potential energy function. A new Monte Carlo method is proposed, group action Markov chain Monte Carlo (GA-MCMC), which augments more conventional trial moves (e.g. random jumps, hybrid Monte Carlo, etc.) with the application of a group action from a well-chosen generating set of the discrete symmetry group; the result is a framework for symmetry-adapted MCMC. It is shown that conventional trial moves are generally optimal for "local mixing" rates, i.e. sampling a single energy well; whereas the group action portion of the GA-MCMC trial move allows the Markov chain to propagate between energy wells and can vastly improve the rate of "global mixing". The proposed method is compared with standard jumps and umbrella sampling (a popular alternative for energy landscapes with barriers) for potential energies with translational, reflection, and rotational symmetries. GA-MCMC is shown to consistently outperform the considered alternatives, even when the symmetry of the potential energy function is broken. The work culminates by extending GA-MCMC to a clustering-type algorithm for interacting dielectric polymer chains. Not only does GA-MCMC again outperform the considered alternatives, but it is the only method which consistently converges for all of the cases considered. Some new and interesting phenomena regarding the electro-elasticity of dielectric polymer chains, unveiled via GA-MCMC, is briefly discussed.

# Contents

Ι	Introduction	2
II	Discrete symmetries, energy barriers, and group theoretic trial moves	6
	II.A The Ising model and clustering algorithms	6
	II.B Group theoretic approach to sampling, GA-MCMC	7
II	I Double-well potential: a first example	8
IV	Translational, reflection, and rotational semi-symmetries	14
	IV.A Translations in 1D	14
	IV.B Octohedral, $\mathcal{D}_{4h}$ , and $\mathcal{D}_{2h}$ symmetries	19
	IV.C Summary and generalizations	20

Email address: matthew.grasinger.1@us.af.mil (Matthew Grasinger)

V	Diel	ectric polymers with monomer-monomer interactions	22
	V.A	Statistical mechanics formulation	22
	V.B	Semi-symmetries and energy barriers	24
	V.C	Group-theoretic clustering of dielectric polymers	25
	V.D	Verification and results	26
<b>3</b> 7 1	I Can	clusion	29
V	ιcon	CIUSIOII	- 48

#### I. Introduction

Numerical integration is of fundamental importance, but is nontrivial in many cases of interest because of the so-called "curse of dimensionality". The curse of dimensionality arises from the fact that, when using numerical quadrature (e.g. Newton-Cotes, Gaussian, etc.), the number of integration points needed to obtain a desired accuracy scales exponentially with the dimension of the domain of integration. When taking expectations, for instance, with over hundreds or thousands of random variables, numerical quadrature is generally infeasible. In contrast, the convergence rates of Monte Carlo methods for stochastic integration are generally independent of dimension. Monte Carlo methods are amenable to approximating solutions to problems that allow a probabilistic interpretation. They have vast applications in uncertainty quantification [42, 75–77, 79, 95], Bayesian statistics [20, 32, 42, 55, 93, 95] (and machine learning [4, 95], more broadly), and computational physics [2, 3, 10, 20, 31, 44, 45, 50, 53, 54, 56, 62, 63, 73, 80, 82, 83, 87, 90, 91]. While the focus of this work will be on equilibrium statistical mechanics, the proposed method for accelerated importance sampling is not specific to physical applications. This work will attempt to make connections with uncertainty quantification and Bayesian inference when appropriate.

Monte Carlo methods have had a lasting success in studying statistical physics. To name a few, Monte Carlo simulation has found applications in binary alloys, quasicrystals, diffusion limited aggregation, liquid-gas transitions, micelle formation, simple and complex fluids, magnetic materials, adsorbed surface layers, polymers, and protein folding [2, 38, 51, 53, 56, 87]. Monte Carlo simulation has also become a pivotal tool for studying phase transitions [30, 56]. The Monte Carlo method which is the focus of this work is the Markov chain Monte Carlo method (MCMC). This work is organized as follows:

- Next some notation and the fundamentals of MCMC are briefly introduced.
- Before closing the introduction, state of the art MCMC techniques for accelerating convergence and
  ensuring accurate approximations—with a focus on those advances which are most relevant to sampling
  potential energy landscapes with energy barriers—are reviewed.
- Section II begins by illustrating how discrete symmetries in the potential energy often lead to energy barriers. It then develops a group-theoretic method for generating trial moves: group action Markov chain Monte Carlo (GA-MCMC).
- Section III compares standard MCMC, umbrella sampling, and GA-MCMC, for sampling a double well potential energy which has an approximate reflection symmetry about x = 0. The results are discussed in detail and chain trajectories are compared. Notions of simulation accuracy and rate of convergence are motivated and defined.
- Section IV generalizes the proposed method to various discrete symmetries which include translations, reflections, and rotations. It also generalizes to problems in higher dimensions. The newly developed sampling approach is shown to exhibit excellent accuracy and convergence properties for all of the examples considered.
- Section V extends the newly developed GA-MCMC to clustering-type algorithms. The extended method is then applied to studying dielectric polymer chains. First the method is verified using a special case for which an exact solution exists. GA-MCMC is then shown to consistently outperform the other sampling approaches considered; and newly unveiled physics are briefly discussed.
- In section VI, the work concludes with a summary of its main ideas and contributions. A perspective is given on the future outlook for this work.

Let x denote a microstate of the ensemble of interest and let  $\Gamma$  denote the phase space of the ensemble; that is, the space of all possible microstates. Assume that  $\Gamma$  is continuous. Then we denote the probability

density of a microstate as  $\pi(x)$  such that  $\pi(x) dx$  is the probability of the system being in  $[x, x + dx] \subset \Gamma$ . We are interested in averages of observables, O, over phase space which we denote by

$$\langle O \rangle \coloneqq \int_{\Gamma} dx \, \pi(x) \, O(x) \,.$$
 (I.1)

MCMC consists of randomly generating a chain of microstates,  $C = \{x_1, ..., x_K\}$ , and then making the approximation

$$\langle O \rangle \approx \langle O \rangle_{\mathcal{C}} := \frac{1}{\mathcal{K}} \sum_{I=1}^{\mathcal{K}} O(x_I)$$
 (I.2)

If the chain of states is properly generated, then  $\langle O \rangle_{\mathcal{C}} \to \langle O \rangle$  as  $\mathcal{K} \to \infty$ . Let

$$C_{x,dx} := \{ x \in C : x \in [x, x + dx] \}. \tag{I.3}$$

Then we desire to sample microstates with the Markov chain such that 1)

$$\left|\mathcal{C}_{x,\mathrm{d}x}\right|/\mathcal{K} \approx \pi\left(x\right)\mathrm{d}x$$
 (I.4)

for all  $x \in \Gamma$ ; and, further, 2) the goal is that the approximation error vanish as quickly as possible. One way to guarantee '1)' is to ensure that the chain is Markovian (i.e. memoryless), ergodic (i.e. can reach all of  $\Gamma$  and is acyclic), and satisfies detailed balance [73]:

$$\pi(x) p(x \to y) = \pi(y) p(y \to x), \qquad (I.5)$$

where  $p(x \to y)$  is the probability of transitioning from state x to y. How to ensure the approximation error vanish as quickly as possible is a much more subtle detail and the problem of interest in this work.

To precisely describe the challenge posed by energy landscapes with barriers, let us formalize the transition step. Each transition step is decomposed into two parts: 1) proposing a trial move and 2) accepting or rejecting the trial move. If the trial move is rejected, the chain is stationary, i.e.  $x \to x$ . Let  $t(x \to y)$  denote the probability of proposing a trial move from state x to y and  $a(x \to y)$  denote the probability of accepting the trial move  $x \to y$ . Let us choose to prescribe the trial and acceptance move probabilities such that they are independent:

$$p(x \to y) = t(x \to y) a(x \to y). \tag{I.6}$$

Then detailed balance can be satisfied by the Metropolis-Hasting acceptance criteria:

$$a(x \to y) = \min \left\{ 1, \frac{\pi(y)}{\pi(x)} \underbrace{\frac{t(y \to x)}{t(x \to y)}}_{=\mathcal{H}(y \to x)} \right\}, \tag{I.7}$$

where  $\mathcal{H}(y \to x)$  is the Hastings factor. One of the most common choices for  $t(x \to y)$  is to prefer relatively small perturbations—which are referred to herein as "standard jumps". Standard jumps generally have an inversion symmetry; that is,  $t(x \to y) = t(y \to x)$  for all x and y. In this case, the Hastings factor is always 1. Let  $y = x + \Delta x$ . Common choices for the distribution of  $\Delta x$  are an anisotropic Gaussian form (centered at  $\Delta x = 0$ ) [5, 20] and trial jumps which are uniformly distributed on  $[-\Delta x_{\text{max}}, \Delta x_{\text{max}}]$  [53].

In the canonical ensemble (i.e. thermodynamic systems in a heat bath at fixed temperature T) the probability of a microstate, x, is proportional to the Boltzmann factor,  $\pi(x) \propto \exp[-\beta U(x)]$ , where U(x) is the potential energy, and  $\beta = 1/k_BT$ . One of the goals of sampling is that the chain mixes rapidly, i.e. move through the support of the probability distribution function rapidly. When rapid mixing occurs, the approximation of expectation values also converge rapidly. However, standard jumps will not mix rapidly when regions of higher probability densities are disconnected and separated by regions of lower probability densities. In the canonical ensemble, lower energy regions correspond with higher probability density and vice versa. As stated in Tuckerman [87],

One of the most challenging computational problems met by researchers in statistical mechanics is the development of methods capable of sampling a canonical distribution when the potential energy is characterized by a large number of local minima separated by high barriers.

This work aims to further address that challenge.

Optimal standard jumps and adaptive Markov chain Monte Carlo. If the sizes of the standard trial jumps are too large, then there may be large increases in energy,  $U(y) - U(x) \gg 0$ , and subsequently the trial jumps will often be rejected. The chain will be mostly stationary. Whereas if the sizes of the trial jumps are too small, then the acceptance rate of trial moves will be higher, but the Markov chain will mix slowly through  $\Gamma$ . It has been established both theoretically [20, 33, 71, 74] and empirically [2, 31, 53, 71, 87] that an acceptance rate of between 20% and 50% is generally optimal <sup>1</sup>. However, how to tune the trial distribution of standard jumps (e.g. the covariance matrix of Gaussian jumps or  $\Delta x_{\text{max}}$  of uniformly distributed jumps) to achieve an optimal acceptance rate is problem dependent. In order to avoid the tediousness of trial and error, practitioners will often track the acceptance rate of the chain and periodically decrease the average jump size if the acceptance rate is below a certain threshold and increase the average jump size if the acceptance rate is above a certain threshold [20, 53]. Although, in this case, the chain is not strictly memoryless (i.e. Markovian), one can show that the chain is still guaranteed to converge to the underlying distribution (I.4), provided that the average jump size ceases to be updated after a finite amount of steps [20]. Throughout this work, an adaptive standard jump size is implemented which adjusts to keep the convergence rate between 15% and 45% for each of the various sampling methods considered. In most cases, the jump size ceased to be adjusted within the first 1000 - 10000 steps; in every case, the jump size adjustment ceased before the simulation ended. As we will see later on, while an adaptive jump size can be an effective means of accelerating convergence, it is not (alone) an effective strategy for mitigating the presence of energy barriers.

Hybrid (or Hamiltonian) Monte Carlo. First introduced in Duane et al. [28], hybrid Monte Carlo generates more intelligent trial moves by taking advantage of the fact that Hamilton's equations conserve energy [1, 14, 31, 87]. At each step, particle velocities are sampled from the Maxwell-Boltzmann distribution and trial moves are generated by integrating Hamilton's equations of motion. A potential advantage of hybrid Monte Carlo is that, because energy does not need to be exactly conserved, the time step for integrating the equations of motion can be greater than conventional molecular dynamics. In fact, an optimal choice of time step is important factor for the efficiency of hybrid Monte Carlo. If the time step is too large, the acceptance rate may be too small; whereas, if the time step is too small, the simulation provides little advantage over molecular dynamics [31]. Theoretical results for specifying the optimal step sizes have been obtained recently [12, 13]. (The analog to hybrid Monte Carlo in for applications in statistics is called "Hamiltonian Monte Carlo"—the distinction is necessary because the temperature is artificial in this case [13, 14, 20].) While hybrid Monte Carlo is an important sampling method for many applications, it also struggles with energy landscapes consisting of multiple wells separated by large barriers [87]. In molecular dynamics simulations, traversing an energy barrier is a "rare event"—meaning the equations of motion need integrated for a significant amount of time before the barrier is crossed. Hybrid Monte Carlo is not commented on further in this work except to remind the reader that many of the sampling methods in MCMC are modular and versatile. By this it is meant that most sampling methods are not mutually exclusive; in principle, hybrid Monte Carlo could be used in tandem with the group-theoretic approach to be proposed in this work.

**Umbrella sampling.** Umbrella sampling is an alternative approach for sampling energy landscapes with barriers [10, 31, 50, 54, 63, 82, 83] (See also,  $\S11$  of [20] for the statistics perspective). The main idea in umbrella sampling is to introduce a pseudopotential in order to reduce or cancel the barriers in the landscape. In other words, the probability distribution is biased by a weight function which depends on the configuration, x:

$$\pi'(x) \propto w(x) \exp(-\beta U(x))$$
. (I.8)

 $<sup>^1</sup>$ In [33], they focus on the scale of the "optimal symmetric jumping kernel" and find that its scale is approximately  $2.4/\sqrt{d}$  where d is the dimension of the space. In the limit of  $d \to \infty$ , this recovers the well-known result that  $\approx 23\%$  is the optimal acceptance ratio for trial moves. More recent work [74] has built upon this by deriving explicit formulae for algorithm efficiency and acceptance rates as functions of the scaling parameter. In practice, however, the differences in the 20% to 50% range are minimal [87]—at least for most applications of interest in statistical physics.

Then the thermodynamic state variables can be obtained by a modified averaging over the MCMC samples:

$$\langle O \rangle \approx \frac{\langle O/w \rangle_{C'}}{\langle 1/w \rangle_{C'}}.$$
 (I.9)

where  $\langle . \rangle_{\mathcal{C}'}$  denotes the chain average obtained by sampling using the modified probability distribution,  $\pi'(.)$ . There are many subtleties related to choosing an appropriate weight function w(x) such that the MCMC sampling is ergodic (i.e. does not become trapped in some subset of  $\Gamma$ ) and has a good convergence rate [10, 20, 31, 63]. By introducing a psuedopotential, Umbrella sampling enhances the rate of (global) mixing at the expense of sampling by importance; in other words, while the pseudopotential allows the chain to traverse energy barriers, it does so by biasing the sampling toward higher energy (and, hence, lower probability density) states. As a consequence, the chain spends more iterations sampling regions of  $\Gamma$  which are less important in the sense that they have smaller contributions to phase averages. Nonetheless umbrella sampling has proven to be an effective sampling approach for energy landscapes with barriers. In the examples that follow, the results from GA-MCMC will be compared to results obtained via umbrella sampling.

Replica exchange (a.k.a. simulated tempering or parallel tempering). Replica exchange is a versatile and promising method for sampling energy landscapes consisting of multiple local minima separated by high barriers [31, 34, 35, 56, 59, 61, 87]. Replica exchange consists of simulating multiple different systems with different thermodynamic states. The most popular forms of replica exchange are also known as simulated tempering or parallel tempering, as the thermodynamic states differ by temperature. The basic idea of simulated tempering is to take advantage of the fact that systems at higher temperature will more readily traverse energy barriers. In addition to the in-simulation trial moves of choice (e.g. standard jumps, hybrid Monte Carlo, etc.), there is also the opportunity to "swap" states between replica systems. Swaps between a high temperature system and a low temperature system have a low probability of being acceptance; thus, the strategy is to make swaps between systems which are nearer to each other in temperature. The thought is that higher temperature systems generate a larger variety of states which then naturally filter toward various wells in the lower temperature systems as the states propagate down through temperature levels. The price, of course, is that it is more computationally expensive to simulate multiple replicas of a given system. Further, the likelihood of accepting exchanges between systems relies on their temperature difference remaining small. Thus, there is a trade-off between the acceptance rate of system exchanges and the total number of replicas—and, hence, overall cost. While problem and parameter dependent, it has been shown that the gain in efficiency from simulated tempering can more than offset the increased cost of tracking multiple systems and exchanging coordinates between them [31, 56, 87]. However, there are many natural questions which arise regarding simulating tempering: 1) How many replica systems should one choose? 2) How should the temperatures (or other system parameters) vary between the systems? 3) Is it better to do replica exchanges more or less frequently? and 4) How does the error compare to that of independent simulations where no exchanges take place? [20, 56]. Recent theoretical results suggest the replica exchange scheme should be specified such that the acceptance rate of swaps is approximately 23% [6]. Exactly how this acceptance rate is achieved, however, is still an open question (at least to the author's knowledge). There are a number of different parameters which must be tuned for replica exchange and it is not always clear how to best tune them. As a result, a direct comparison of replica exchange with the group-theoretic approach is forgone.

Group theoretic acceleration in particle-scale methods. This work is inspired, in part, by the successes of various works which leverage group theory in order to improve the efficiency of modeling bulk materials, nanostructures, viruses, etc., using molecular dynamics [25, 29, 48, 92] and the Boltzmann equation [25]. Similar considerations of geometry and symmetry transformations have also been leveraged to develop various clustering-type MCMC algorithms [27, 47, 58, 70]. An aim of this work is to explore geometry and symmetry in the context of MCMC more broadly (e.g. field-interactions, potentials with symmetry, etc.) using group theory and with an emphasis on the importance of discrete symmetries.

# II. Discrete symmetries, energy barriers, and group theoretic trial moves

#### II.A. The Ising model and clustering algorithms

As an illustration, let us consider the Ising model for ferromagnetism. In this model, there is a lattice of spin states, either spin-up or spin-down, which interact with their nearest neighbors. Generally, the allowable spin states are represented by  $\mu_i = \pm 1$  for i = 1, ..., n where n is the number of spins in the lattice and  $\Gamma = \{-1, 1\}^n$ . Assume there is not an externally applied magnetic field. Then the potential energy is

$$U = -J \sum_{(i,j)'} \mu_i \mu_j, \tag{II.1}$$

where J is the strength of interactions and the notation (i,j)' is used to indicate that the sum is over all pairs such that i and j are nearest neighbors. Assuming J > 0, microstates with a greater number of neighboring like spins are more likely than microstates with lesser numbers of neighboring like spins. In particular, the two states with the greatest probability occur when all of the spins in the lattice are up and when all of the spins are down. However, these two greatest probability states are separated by many lower probability states in the sense that transitioning from one state to the other requires flipping all of the spins in the lattice. As  $\beta J \to \infty$ , the probability of the separating states vanishes exponentially. A Markov chain consisting of trial moves where only a single spin is flipped would therefore mix very slowly, leading to slow convergence. This phenomena is called critical slowing down [53, 91].

Clustering algorithms represented a breakthrough in mitigating the critical slowing down of the Ising model near the phase transition temperature [80, 90, 91]. Notably, clustering exploits what is approximately a discrete symmetry in the potential energy landscape of the Ising model: a state with a large cluster of like spins <sup>2</sup> has approximately the same energy when all of the spins in the cluster are flipped to the opposite sign–provided that the interior of the cluster is large "enough" relative to the boundary. Clustering bypasses many of the lower probability separating states and allows rapid mixing to occur.

The Ising model and associated clustering algorithms are a special case of a more general principle: discrete, approximate symmetries of a potential energy landscape often lead to multiple energy wells separated by energy barriers. Further, mixing and convergence of the MCMC method can be accelerated by leveraging (i.e. sampling) what is known about the approximate symmetries of the system. Let the approximate symmetry be described by the group  $\mathcal{G}$  and let  $\rho: \mathcal{G} \times \Gamma \mapsto \Gamma$  be a faithful group action on  $\Gamma^3$ . For brevity, I will use  $g \cdot x$  to denote  $\rho(g, x)$ . Let us say a potential energy is *semi-symmetric* provided

$$U(x) = U_{\mathcal{G}}(x) + \epsilon U_{0}(x) \tag{II.2a}$$

where  $\epsilon$  small enough and

$$U_{\mathcal{G}}(x) = U_{\mathcal{G}}(g \cdot x) \tag{II.2b}$$

for all  $g \in \mathcal{G}$ . Provided  $U_{\mathcal{G}}$  is not constant, there exists a local minima of  $U_{\mathcal{G}}$  which we denote by  $x^{*-4}$ . Assume  $\mathcal{G}$  is discrete. Then, by (II.2b),  $g \cdot x^{*}$  is also a local minima for each  $g \in \mathcal{G}$ . If  $|\mathcal{G} \cdot x^{*}| > 1$ , where

$$\mathcal{G} \cdot x^* = \{ g \cdot x^* : g \in \mathcal{G} \} \tag{II.3}$$

is the orbit of  $x^*$ , then  $U_{\mathcal{G}}$  has multiple energy wells (i.e. multiple local minima). As an illustration, assume  $U_{\mathcal{G}}(x^*) \leq U_{\mathcal{G}}(x)$  for all  $x \in \Gamma$  and consider the limit of  $\beta \to \infty$  and  $\epsilon \beta < \infty$ . If the maximum size of trial jumps is less than

$$\sup_{x \in \mathcal{G} \cdot x^*} \left( \inf \left\{ |x - x'| : x' \in \mathcal{G} \cdot x^*, x' \neq x \right\} \right)$$
 (II.4)

then the standard method for trial propositions will result in a chain that is not ergodic. The chain becomes

<sup>&</sup>lt;sup>2</sup>By cluster, we mean a group of lattice sites that are connected through a series of neighbors.

<sup>&</sup>lt;sup>3</sup>By "faithful" it is meant that, for each  $g \in \mathcal{G}$ ,  $g \neq e$ , there exists some  $x \in \Gamma$  such that  $\rho(g, x) \neq x$ .

<sup>&</sup>lt;sup>4</sup>If  $\Gamma$  is not compact,  $x^*$  may not be contained within  $\Gamma$ . However, it is guaranteed that there is some neighborhood of  $x^*$  which is an energy well and has nonempty intersection with  $\Gamma$  such that the proceeding arguments still hold.

frozen in a small neighborhood of some  $x^{**} \in \mathcal{G} \cdot x^*$  with probability 1; while it may be possible to transition to another  $x \in \mathcal{G} \cdot x^*$ , the probability of this occurring is 0; and, lastly, by (II.4), it is not possible for the chain to transition to all  $x \in \mathcal{G} \cdot x^*$ . Although the chain does not freeze when  $\beta$  is large but finite, it is evident that the standard MCMC will suffer from critical slowing down. The rate at which the chain mixing slows down, as a function of  $\beta$  and  $\epsilon$ , will vary by the different forms of  $U_{\mathcal{G}}$  and  $U_{0}$ .

#### II.B. Group theoretic approach to sampling, GA-MCMC

Here a modification to the standard method for trial move propositions is proposed given some knowledge of  $\mathcal{G}$ . The group  $\mathcal{G}$  may be infinite. Let  $\langle\langle S\rangle\rangle$  denote the group generated by the set S (here double angle brackets are used, as opposed to the more standard notation of single angle brackets, in order to distinguish group generation,  $\langle\langle . \rangle\rangle$ , from ensemble averaging,  $\langle . \rangle\rangle$ . Take some generating set, G, of the group G (i.e.  $\langle\langle G\rangle\rangle = G$ ) such that

- 1)  $e \in G$ ; that is, it can be stationary, and
- 2) G contains the inverse of each of its elements (i.e.  $g \in G \iff g^{-1} \in G$ ); that is, the generating set is "reversible".

Then assign probabilities,  $\omega_i > 0$ , to each  $g_i \in G$  such that  $\omega_1 + \omega_2 + \cdots + \omega_{|G|} = 1$ . Mixing is accelerated by randomly sampling a group element from G (consistent with their prescribed probabilities) and applying its action to the current microstate as part of the trial move. This way if the chain is local to some energy well, it can efficiently mix to other wells in the potential energy landscape—even when  $\beta \gg 1$ . The basic idea, in general, is to propose a trial move by 1) a standard jump and then 2) applying a randomly sampled group action to the perturbed state. As a concrete example, assume the thermodynamic system consists of n particles and that the state of each particle is described by a point  $x_i$  in a manifold, X (such that  $\Gamma = X^n$  and  $x = (x_1, \ldots, x_n)$ ) 5. An outline of the transition process for the Markov chain is as follows:

- 1) Randomly choose a particle index, i, in  $\{1, 2, ..., n\}$ .
- 2) Sample a jump (i.e. perturbation)  $\Delta x_i$  in  $\{\Delta x \in X : |\Delta x| \leq \Delta x_{max}\}$  where  $\Delta x_{max}$  is the maximum step size of a jump.
- 3) Set the trial move:

$$x_{\tau} = (x_1, \dots, x_i + \Delta x_i, \dots, x_n)$$

where x is the current state of the chain and  $x_{\tau}$  is the trial move.

- 4) Sample a group element,  $g_j \in G$ , consistent with the probabilities  $\omega_1, \ldots, \omega_{|G|}$ .
- 5) Propagate the trial move via the group action:  $x_{\tau} \to g_i \cdot x_{\tau}$ .
- 6) Accept or reject the trial move based on the Metropolis-Hastings acceptance criteria, (I.7).

Here steps 1-3 ensure that the chain mixes locally; that is, it allows the chain to properly sample an individual energy well. Steps 4 and 5 ensure that the chain mixes globally; i.e., it ensures the chain does not end up localized to a proper subset of the energy well(s). If one makes the analogy of MCMC sampling with random walks and diffusion, then the proposed sampling approach can be thought of as a kind of multiscale or multimodal diffusion where steps 1-3 represent diffusion at the smaller scale and steps 4 and 5 represent diffusion at larger scales. It will be shown by example that, for discrete semi-symmetric energy landscapes, the above transition process can significantly improve the rate of convergence over standard MCMC approaches and even outperform umbrella sampling. Note that, for simplicity, the procedure was outlined for  $U = U_{\mathcal{G}} + \epsilon U_0$ , but, in general, it may also possible to make more complicated decompositions, e.g.

$$U = U_{G_1} + U_{G_2} + \dots U_{G_n} + \epsilon U_0 \tag{II.5}$$

and then sample from  $G = G_1 \cup G_2 \cup \cdots \cup G_n$  where  $\langle \langle G_i \rangle \rangle = \mathcal{G}_i$ . In this case, it may be necessary to scale the sampling weights according to the energy scales of each of the  $U_{\mathcal{G}_i}$ .

While the probabilities which are optimal for the convergence rate may vary by  $U, U_{\mathcal{G}}, \epsilon, U_0$ , and  $\beta$ , we find that the simple choice of  $\omega_1, \ldots, \omega_{|G|} = 1/|G|$  works well for the examples considered in this work. This choice is motivated by the assertion that  $U_{\mathcal{G}}(x) = U_{\mathcal{G}}(g \cdot x)$  for all  $g \in \mathcal{G}$  and the assumption that  $\epsilon$  is small.

<sup>&</sup>lt;sup>5</sup> For clarity, chain samples are indexed by uppercase letters and particle states are indexed by lowercase letters.

In this case, all microstates in  $\mathcal{G} \cdot x$  are approximately equally likely. Thus, in order for our Markov chain to converge to the underlying probability distribution as quickly as possible, it makes sense to transition between these states with equal probability. This choice has the added benefit of simplicity in that it ensures that the Hastings factor is always 1.

Before moving on to examples of using the newly proposed sampling technique to model the statistical mechanics of various systems, I pause to sketch how the above developments can be generalized to other applications of MCMC methods. While the above discussion was framed in terms of energy landscapes and energy barriers, the principles extend to any case in which a probability distribution with discrete semi-symmetries is being sampled. In this broader sense, energy wells are analogous to regions of the domain of the random variable(s) which have a greater likelihood, and energy barriers correspond with regions that have a lesser likelihood. Using Bayesian inference as an example (see [18, 20, 32, 75, 93]), the same transition process can be used when the posterior probability distribution is discretely semi-symmetric.

As mentioned previously, there has been recent work on leveraging symmetry and group theory to accelerate other types of particle-scale models [9, 25, 29, 36, 48, 92]. However, many of these methods rely on the corresponding symmetry or group structure to be exact (i.e. the special case of  $\epsilon = 0$ ). One of the principal advantages of the method proposed in this work is that it accelerates the computation for more generic problems; that is, cases where  $\epsilon$  can be finite and is only required to be "small enough". A topic of interest for future work would be to conduct an analysis which relates the rate of convergence as a function of  $\beta$  and  $\epsilon$  given some properties of the energy landscape: namely, U,  $U_{\mathcal{G}}$ , and  $U_0$ . Further, note that the decomposition of U into  $U_{\mathcal{G}}$ ,  $\epsilon$ , and  $U_0$ , is generally nonunique. An additional potential advantage of such an analysis would be to elucidate which choice of decomposition may be more or less desirable given certain conditions.

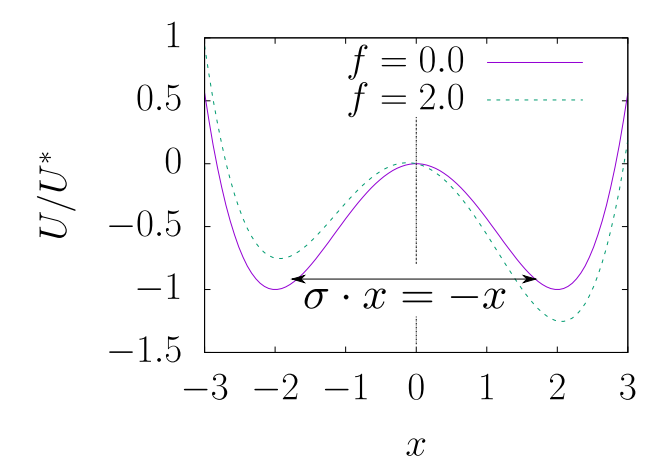
# III. Double-well potential: a first example

A single degree of freedom system,  $x \in \mathbb{R}$ , in a double well potential given by

$$U = ax^4 - bx^2 - fx (III.1)$$

is considered. The potential energy, U, has a reflection symmetry about x=0 when f=0. It is semi-symmetric when f is small enough. To be precise,  $U_{\mathcal{G}}(x)=ax^4-bx^2$ ,  $\epsilon=f$ , and  $U_0(x)=-x$ . The symmetry of  $U_{\mathcal{G}}$  is described by the dihedral group  $\mathcal{D}_1$  with action  $\rho(\sigma,x)=\sigma\cdot x=-x$ . Thus, the standard jump part of trial propositions is augmented by sampling  $g\in\{e,\sigma\}$  where each element has probability 1/2 and applying the action  $x\to g\cdot x$ . The energy landscape, its symmetry, and the effect of breaking its symmetry (f>0) are shown in figure 1. Some simple examples of energies with reflection symmetry are 1) charged particles interacting with the field induced by a dipole in 2D, and 2) the interaction of liquid crystals with a local director field [26].

Given the potential energy, (III.1), let us first consider the case where a=1,b=8, and f=0 such that the landscape is strictly symmetric. The initial mixing of Markov chains that utilize a standard sampling approach, the group-theoretic-based sampling approach, and umbrella sampling with  $w(x) = \exp\left(-\tilde{b}x^2\right)$  is shown in figure 2. Here  $\tilde{b}=4$  so that the effective potential of the umbrella sampling approach is  $x^4-4x^2$ . Figure 2.a and figure 2.b show the initial chain trajectories for the first 1000 steps, sampled every 20 steps, and the first 10000 steps, sampled every 200 steps, respectively. The state of each chain is given by the x-axis and the y-axis signifies the progression of the chain; that is, the number of steps the chain has taken increases with y. The trajectories for the standard MCMC sampling approach are depicted by a solid purple line and '+' markers, the group-theoretic-based sampling trajectories are depicted by a dashed green line and 'x' markers, and the umbrella sampling trajectories are depicted by a blue dash-dot line and '\* markers; for reference, the potential energy is plotted on the second y-axis. It can be seen that the potential energy consists of two energy wells at  $x=\pm 2$ . For the first 1000 steps, the standard sampling approach moves to the left energy well and is then localized near the local minima, x=-2. The chain trajectory obtained



Var.	Value
$\Gamma$	$\mathbb{R}$
$U_{\mathcal{G}}$	$ax^4 - bx^2$
$\epsilon U_0$	-fx
${\cal G}$	$\mathcal{D}_1$
G	$\{e,\sigma\}$
$\omega_i$	$\omega_1 = \omega_2 = 1/2$
$\ell^*$	$\sqrt{b/2a}$ $b^2/4a$
$U^*$	$b^2/4a$

Figure 1: Double well energy and reflection action. Double well potential energy given by  $U=ax^4-bx^2-fx$  where a=1, b=8, and f=0 (solid line) and f=2 (dashed line). The potential energy has a reflection semi-symmetry about x=0; an example of its action,  $\sigma \cdot x$ , is also shown.

Table 1: Properties of the double well thermodynamic system and its associated group-theoretic sampling approach.

via umbrella sampling also moves quickly into the left energy well <sup>6</sup>. However, because the pseudopotential biases the chain toward x = 0, the umbrella chain, though localized in the left well, is concentrated about some x > -2. By step 10000, the standard chain still has not mixed to the right energy well. The biasing of the umbrella chain has allowed it to traverse the energy barrier and mix between the wells after a sufficient amount of steps. In figure 2.b, this has occurred at approximately 2000 steps. In contrast, figure 2.a shows that the group-theoretic chain has traversed the barrier several times and mixed well throughout the support of  $\pi(x)$  within the first 200-300 steps.

Figure 2.c and figure 2.d show histograms of the normalized density of chain samples for the standard (solid purple), umbrella (singly hatched green), and group-theoretic (doubly hatched blue) sampling approaches after 1000 steps and 10000 steps, respectively. The probability density  $\pi(x)$  as calculated by high fidelity numerical quadrature is overlaid for comparison. As expected (from observations made regarding the chain trajectories), the density of samples for the standard and umbrella sampling approaches are overly biased toward the left energy well after 1000 steps. In contrast, the group-theoretic approach approximates  $\pi(x)$  reasonably well after only the first 1000 steps and is nearly exact after 10000. After 10000 steps, the umbrella chain has mixed to the second well and approximately resembles the two-peak quality of the exact distribution. However, it is important to note that the peaks with the largest density of samples for the umbrella chain are centered at approximately  $x = \pm 1.5$  and thus are offset from the peaks of the exact distribution  $(x = \pm 2)$ . This is to be expected because the umbrella sampling consists of a pseudopotential which biases the chain towards x=0; indeed, this is how the chain is able to mix into the second energy well in a finite number of steps. In approximating ensemble averages using umbrella sampling, equation (I.9) corrects for the fact that the umbrella chain is not sampling the exact distribution. However, because the biasing of the pseudopotential causes the chain to more densely sample regions of  $\Gamma$  with lower  $\pi(x) dx$ , the ensemble averages approximated by the umbrella sampling approach will often have a slower convergence rate. This is one of the principal drawbacks of umbrella sampling. If the pseudopotential is greater, the chain can mix more rapidly between wells but does not densely sample regions of greatest  $\pi(x) dx$ ; that is, the global mixing comes at the expense of sampling based on importance. If the pseudopotential is lesser, then the chain becomes trapped in a subset of  $\Gamma$  and may not sample the full support of  $\pi(x)$ .

<sup>&</sup>lt;sup>6</sup>It is merely a coincidence that both the standard and umbrella chains begin by moving into the left well. Both approaches were equally likely to begin by moving into the right well.

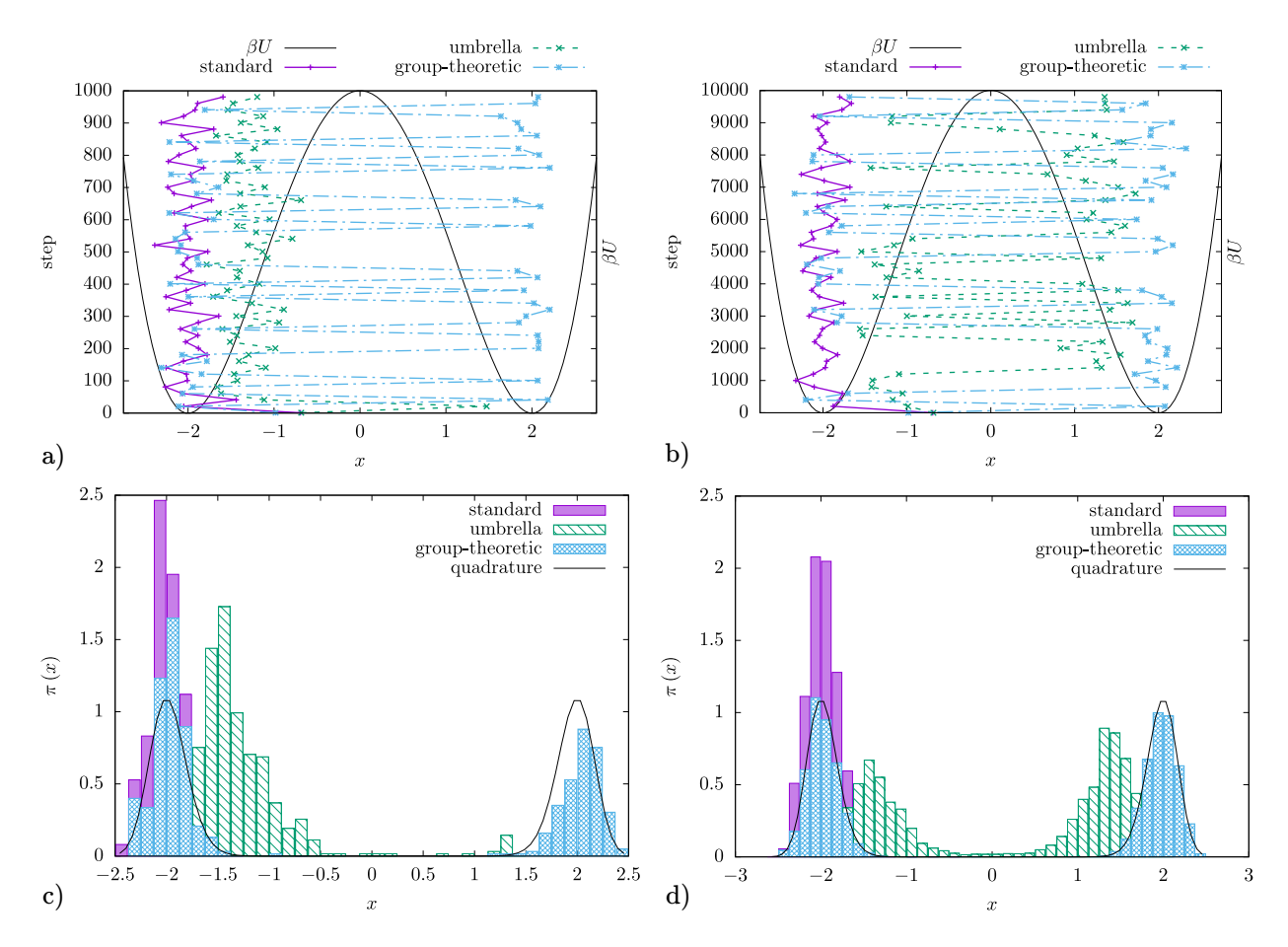


Figure 2: Markov chain mixing of the various sampling approaches. a) Markov chain trajectories (sampled every 20 steps) where the x-axis is a snapshot of the chain state, x, and the y-axis corresponds with increasing simulation step. For the first 1000 steps, the standard and umbrella sampling approaches are localized to the left energy well while the group-theoretic approach mixes readily between wells. b) Markov chain trajectories for the first 10000 steps. The standard approach is still localized to a single well. The umbrella approach has mixed between wells but is overly representative of states nearer to x = 0. The group-theoretic approach continues its rapid mixing. c) Histograms of the density of chain samples after the first 1000 steps. The probability density,  $\pi(x)$ , as computed using numerical quadrature, is shown for comparison. The group-theoretic approach is converging rapidly to  $\pi(x)$  whereas its counterparts are overly representative of the left well. d) Histograms of the density of chain samples after the first 10000 steps. The standard approach is still localized to the left well (i.e. is not ergodic). The umbrella approach has mixed (approximately) evenly between the wells but, because of the pseudopotential, has sampled a large density of states which make negligible contribution to expected values of interest. The group-theoretic approach shows excellent agreement with  $\pi(x)$ .

Next let us consider the convergence of chain approximations to ensemble averages. Let

$$\langle O \rangle_K := \frac{1}{K} \sum_{I=1}^K O(x_I)$$
 (III.2)

denote the chain average of an observable O after K steps (i.e. the rolling average at step K). To measure the convergence rate of a sampling approach, 100 MCMC simulations are run for  $K = 10^6$  steps. Let an overline (i.e.  $\Box$ ) denote an average quantity over the simulation population. Then

$$\overline{\left|\langle O\rangle_{K} - \langle O\rangle_{\text{quad}}\right|} = \frac{1}{100} \sum_{\text{over MCMCs}} \left|\langle O\rangle_{K} - \langle O\rangle_{\text{quad}}\right|, \tag{III.3}$$

where  $\langle O \rangle_{\text{quad}}$  is the ensemble average of O using high-fidelity quadrature [11, 88], is used to measure the convergence rate of a given sampling approach for  $\langle O \rangle$ . Figure 3 shows  $|\langle x \rangle_K - \langle x \rangle_{\text{quad}}|/\ell^*$  as a function of K, where  $\ell^* = \sqrt{|b/2a|}$  is the natural unit of length for the system of interest. Figure 3 compares the convergence of  $\langle x \rangle$  for umbrella sampling with  $\tilde{b}=2$ ,  $\tilde{b}=4$ ,  $\tilde{b}=6$  and the group-theoretic sampling approach. Among the umbrella sampling methods, notice that, for the greatest choice of  $\tilde{b}$  (i.e.  $\tilde{b}=6$ ), the error is smallest for the first 1000 steps. In contrast, for the smallest choice of b (i.e. b=2), the error at the outset is greatest (and is near unity) for the first 10000 steps. However, the smaller choices of  $\tilde{b}$  have a greater rate of convergence over the long term (e.g.  $K \ge 100000$ ). This highlights the aforementioned drawback of umbrella sampling: when the pseudopotential is large, the chain mixes rapidly, which leads to a smaller initial error. However, a consequence of the greater pseudopotential is that the chain spends too much time sampling regions of  $\Gamma$  for which  $\pi(x) dx$  is small and hence does not contribute meaningfully to the integral. When the pseudopotential is small, the chain samples regions of greater  $\pi(x) dx$ , i.e. greater importance. However, when regions of greater importance are disconnected, then the smaller pseudopotential results in the chain becoming localized to just one of those regions and not mixing globally. Thus, in many instances, even with detailed knowledge of the exact form of U, the choice for the umbrella sampling pseudopotential is nontrivial; and, in some cases, it may be that there does not exist a pseudopotential which results in a reasonable convergence rate. The group-theoretic approach does not require such a trade-off between global mixing and local importance. Indeed, figure 3 shows that both 1) the initial error of the group-theoretic approach is smaller than all of its umbrella sampling counterparts and 2) its long term convergence is faster than all of its umbrella sampling counterparts. The error curve of  $\langle x \rangle$  for the standard MCMC sampling approach is not shown as its convergence rate is effectively zero. For every one of the 100 simulations, the standard approach is trapped in one of the two wells for the entire simulation of  $10^6$  steps.

Figure 3 shows the error curves for approximating  $\langle U \rangle$  (a) and  $\langle x^2 \rangle$  (b) by standard, umbrella with  $\tilde{b}=2$ , umbrella with  $\tilde{b}=4$ , and group-theoretic sampling approaches. Here,  $U^*=b^2/4a$ . For both  $\langle U \rangle$  and  $\langle x^2 \rangle$ , because of symmetry, the contribution of the integral from the left well is equivalent to the contribution of the integral from the right well. Because of this, the standard sampling and group-theoretic approaches perform quite well and converge rapidly to the solution obtained via high-fidelity numerical quadrature. In contrast, as the pseudopotential of the umbrella sampling increases, both the initial error increases and the long term convergence rate decreases. This is because, for accuracy of  $\langle U \rangle$  and  $\langle x^2 \rangle$ , it is only required that the left or right well be sampled. However, as  $\tilde{b}$  increases, the umbrella chain spends less time sampling either of the two wells and is more concentrated near x=0. To summarize, this first example was explored in some depth and it was found that, for all of the ensemble averages considered, the group-theoretic sampling approach performed as well or better than each of the other options. Next let us consider the effects of breaking the symmetry of U (i.e.  $\epsilon \neq 0$ ) and temperature changes on the accuracy and convergence rates of the various sampling methods.

First, some definitions are made. Let  $\mathbb{O} = \{x, x^2, U, U^2\}$  be the set of observables of interest. Consider figure 3 and figure 4: when the error curves are plotted using a log-log scale, in general—to a good approximation—the error decays linearly. This implies that the error scales like  $K^{\alpha}$ . The exponent,  $\alpha$ , is a measure of the convergence rate and clearly it is desirable that  $\alpha$  be as negative as possible. The calculation

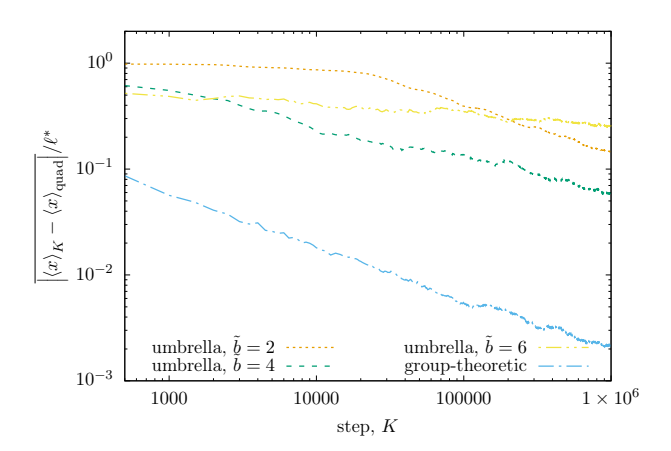


Figure 3: Convergence of  $\langle x \rangle$  for umbrella sampling approaches with  $\tilde{b}=2$ ,  $\tilde{b}=4$ ,  $\tilde{b}=6$  and the group-theoretic sampling approach. Larger  $\tilde{b}$  has a smaller initial error but slower long-term convergence rate; whereas small  $\tilde{b}$  has a larger initial error with faster long-term convergence rate. The group-theoretic approach has no such trade-off: it has a smaller initial error and a faster long-term convergence rate than all of the umbrella variants. The standard sampling approach (not shown) does not show any discernible signs of convergence for the duration of the simulation.

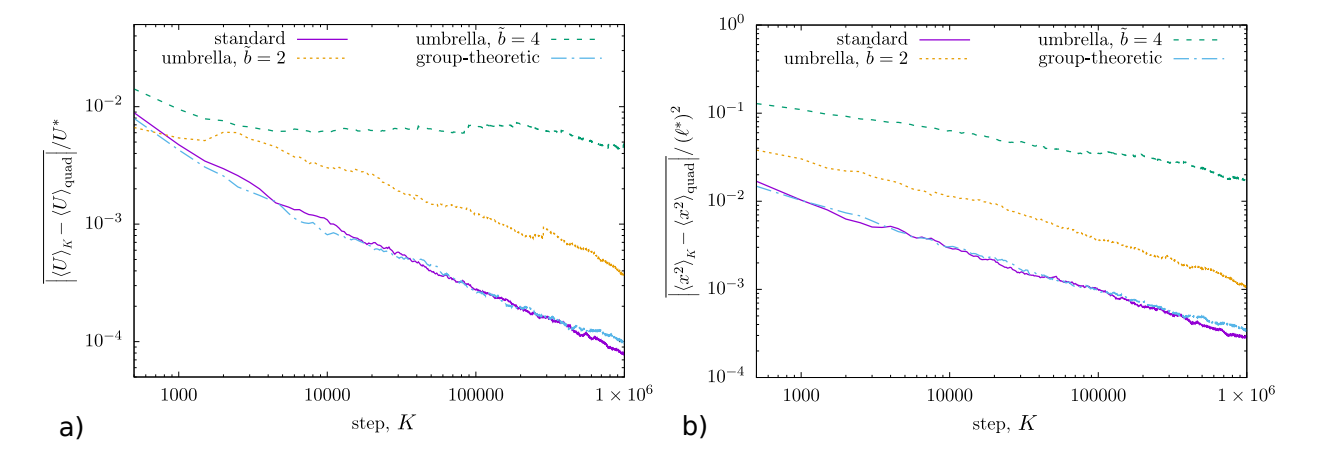


Figure 4: Convergence of a)  $\langle U \rangle$  and b)  $\langle x^2 \rangle$  using standard, umbrella with  $\tilde{b}=2$ , umbrella with  $\tilde{b}=4$ , and group-theoretic sampling approaches. The standard and group-theoretic approaches show superior convergence relative to the umbrella sampling variants. This is because accurate approximations of  $\langle U \rangle$  and  $\langle x^2 \rangle$  can be obtained via sampling one of the two wells and both the standard and group-theoretic approaches have optimal local mixing properties.

	a = 1, t	p = 8, f = 1	$0, \beta = 1.$		$a = 1, b = 8, f = 4, \beta = 1.$				
method	$\min_{O \in \mathbb{O}} \alpha_O$	$\max_{O \in \mathbb{O}} \alpha_O$	$\min_{O \in \mathbb{O}} \mathcal{E}_O$	$\max_{O \in \mathbb{O}} \mathcal{E}_O$	method	$\min_{O \in \mathbb{O}} \alpha_O$	$\max_{O \in \mathbb{O}} \alpha_O$	$\min_{O \in \mathbb{O}} \mathcal{E}_O$	$\max_{O \in \mathbb{O}} \mathcal{E}_O$
SS	-0.7407	-0.0047	+0.0001	+0.9643	SS	-0.7309	-0.7273	+0.0038	+0.0273
US	-0.5559	-0.0256	+0.0001	+0.8866	US	-0.9763	-0.8984	+0.0008	+0.0042
GT	-0.6356	-0.4339	+0.0001	+0.0017	GT	-0.7672	-0.5571	+0.0001	+0.0006
GU	-0.5910	-0.4144	+0.0001	+0.0018	GU	-0.4690	-0.4509	+0.0002	+0.0006
						'			
	a=1, b	= 8, f = 0	$\beta = 10.$			a=1, b	= 8, f = 1	$\beta = 10.$	
method	$\min_{O \in \mathbb{O}} \alpha_O$	$\max_{O \in \mathbb{O}} \alpha_O$	$\min_{O\in\mathbb{O}}\mathcal{E}_O$	$\max_{O \in \mathbb{O}} \mathcal{E}_O$	method	$\min_{O \in \mathbb{O}} \alpha_O$	$\max_{O \in \mathbb{O}} \alpha_O$	$\min_{O\in\mathbb{O}}\mathcal{E}_O$	$\max_{O \in \mathbb{O}} \mathcal{E}_O$
SS	-1.0065	+0.0004	+0.0000	+0.9988	SS	-0.0182	-0.0001	+0.0245	+0.7788
US	-0.7458	+0.0001	+0.0000	+0.9988	US	-0.0077	-0.0001	+0.0220	+0.6989
GT	-0.9880	-0.5025	+0.0000	+0.0018	$\operatorname{GT}$	-1.0023	-0.6435	+0.0000	+0.0001
$\operatorname{GU}$	-0.7939	-0.5064	+0.0000	+0.0018	GU	-0.7691	-0.4717	+0.0000	+0.0001
	1								
	a=1, b	= 8, f = 4	$\beta = 10.$			a = 1/2, t	p = 16, f =	$= 8, \ \beta = 1.$	
method	$\min_{O \in \mathbb{O}} \alpha_O$	$\max_{O \in \mathbb{O}} \alpha_O$	$\min_{O\in\mathbb{O}}\mathcal{E}_O$	$\max_{O\in\mathbb{O}}\mathcal{E}_O$	method	$\min_{O \in \mathbb{O}} \alpha_O$	$\max_{O \in \mathbb{O}} \alpha_O$	$\min_{O\in\mathbb{O}}\mathcal{E}_O$	$\max_{O \in \mathbb{O}} \mathcal{E}_O$
SS	-1.0001	-0.6610	+0.0000	+0.0001	SS	-0.0332	-0.0013	+0.0265	+0.4188
US	-0.8451	-0.5599	+0.0000	+0.0001	US	-0.0103	-0.0002	+0.0190	+0.2991
$\operatorname{GT}$	-1.0074	-0.7553	+0.0001	+0.0001	$\operatorname{GT}$	-1.0114	-0.8101	+0.0001	+0.0002
$\operatorname{GU}$	-0.8390	-0.5218	+0.0000	+0.0001	$\operatorname{GU}$	-0.5473	-0.5363	+0.0000	+0.0002

Table 2: Error and convergence rates for double well potential. Fastest rate of convergence,  $\min_{O \in \mathbb{O}} \alpha_O$ ; slowest rate of convergence,  $\max_{O \in \mathbb{O}} \alpha_O$ ; greatest accuracy,  $\min_{O \in \mathbb{O}} \mathcal{E}_O$ ; and least accuracy,  $\max_{O \in \mathbb{O}} \mathcal{E}_O$ , for each of the sampling approaches considered. The standard (denoted 'SS'), umbrella (with  $\tilde{b} = 4$ , denoted 'US'), group-theoretic (denoted 'GT') and group-theoretic with umbrella ( $\tilde{b} = 4$ , denoted 'GU') sampling approaches are compared. Energy landscapes with various barriers, temperatures, and f are considered.

for  $\alpha_O$  consists of fitting a line (using least squares) to the  $\log |\overline{\langle O \rangle_K - \langle O \rangle_{\text{quad}}}|$  vs.  $\log K$  data. The measure of convergence rate,  $\alpha_O$ , is then the slope of this line. Lastly, for brevity, let  $\mathcal{E}_O := |\overline{\langle O \rangle_K - \langle O \rangle_{\text{quad}}}|/O^*$  denote the sample average of the error after the total  $10^6$  simulation steps.

Table 2 shows min  $\alpha_O$  and max  $\alpha_O$  for each of the sampling approaches considered, which describe the fastest and slowest rates of convergence, respectively, for the observables of interest. Table 2 also shows min  $\mathcal{E}_O$  and max  $\mathcal{E}_O$ , which describe the most accurate and least accurate approximations, respectively. The standard (denoted 'SS'), umbrella (with  $\tilde{b}=4$ , denoted 'US'), group-theoretic (denoted 'GT') and group-theoretic with umbrella ( $\tilde{b}=4$ , denoted 'GU') sampling approaches are compared. Energy landscapes with various barriers and f are considered. The first example (upper left),  $a=1,b=8,f=0,\beta=1$ , is consistent with the discussion regarding figure 3 and figure 4; that is, the standard sampling approach has the least min  $\alpha_O$  (i.e. shows the fastest convergence rate) for some observables while it simultaneously exhibits the slowest convergence rate for others. The standard and umbrella sampling approaches are not robust for this example (i.e. exhibit the greatest maximum  $\mathcal{E}_O$ ), whereas the group-theoretic and group-theoretic with umbrella sampling approaches show good convergence rates and high accuracy.

In the next example (upper right) symmetry is broken and f=4. There the non group-theoretic approaches show faster minimum and maximum convergence rates. The umbrella sampling approach convergences the most rapidly. The performance of the non-group-theoretic approaches improves (for all observables) because, as the force increases for constant a, b, and  $\beta$ , 1) the energy barrier between the two wells is reduced and 2) the right well has a greater contribution to the integral than the left such that mixing between wells becomes less important. Interestingly, however, despite the faster convergence of the non group-theoretic approaches, the group-theoretic approaches still exhibit good convergence rates and have a higher accuracy than their non group-theoretic-based counterparts.

In the next three examples (middle left, middle right, and bottom left), the temperature is lowered  $(\beta=10)$  and the force is gradually increased from f=0 (middle left) to f=1 (middle right) and f=4 (bottom left). The lower temperature further degrades the rate of convergence for the non-group-theoretic approaches relative to the  $f=0, \beta=1$  case; whereas, the convergence rates for the group-theoretic approaches increase. As more force is applied (e.g. f=1 and f=4), the energy landscape, again, becomes less symmetric and both the accuracy and convergence rates of the non-group-theoretic approaches improve. However, in contrast to the  $f=4, \beta=1$  case (top right), the group-theoretic sampling approach convergences at a faster rate than the non-group-theoretic approaches for the  $f=4, \beta=10$  case (bottom left). Thus, the effect of symmetry breaking on which approach performs best also depends on the temperature of the system.

The last example (bottom right) consists of an energy landscape with deeper, more separated wells (a = 1/2, b = 16). Despite the force being greater than all of the previous examples (f = 8), the convergence and accuracy of the non-group-theoretic approaches are still poor. This agrees with intuition: the force required to make non-group-theoretic approaches viable depends on the well depth and well separation of the energy landscape.

To get a better sense of the interplay between well depth, well separation, and the applied force on the robustness of the various sampling approaches, figure 5 shows heat maps of max  $\alpha_O$  (i.e. slowest convergence rate) as a function of b (x-axis) and f (y-axis). Figure 5 compares the standard (top left), umbrella ( $\dot{b}$  = 4) (top right), group-theoretic (bottom left), and group-theoretic with umbrella (bottom right) sampling approaches. For each case,  $\beta = 1$ . At small b and large f, the standard sampling approach has a slightly greater convergence rate than the other sampling approaches. However, there is a line in parameter space, 2b+7=f, where the convergence rate changes dramatically. When 2b+7>f, the convergence rate of the standard sampling approach drops off quickly until the method does not converge (i.e.  $\max \alpha_Q \approx 0$ ). Somewhat non-intuitively, the convergence rate of the standard approach is greatest just before this dropoff; that is, when  $2b+7 \lesssim f$ . This linear relationship does not persist, however, for the entirety of the parameter space. When  $f \gtrsim 13$ , the standard approach converges for some 2b + 7 > f. The effect of umbrella sampling (top right) can be seen upon examination of the line with delineates the region of parameter space for which the method converges from the region of parameter space for which it does not converge. Indeed, the line again begins at b = 7, f = 0 but has a slightly more gradual slope-indicating that umbrella sampling converges for a somewhat larger region of (b, f) space. The trade-off is that the umbrella sampling has slower convergence for 2b + 7 < f. These differences between the standard and umbrella sampling approaches are minor however. Importantly, the group-theoretic approaches (bottom left and bottom right) show a good convergence rate for the whole parameter space considered. This highlights the robustness of the proposed approach for sampling energy landscapes with discrete symmetries and corresponding energy barriers. Interestingly, the convergence rate for the group-theoretic approach (without umbrella sampling) seems to even be improving for large b and f-despite the fact that large f means the energy landscape has a large deviation from the symmetry of  $U_{\mathcal{G}}$ . In the next section, the principles developed here will be generalized to more types of symmetry (e.g. translation, rotation) and higher dimensions.

## IV. Translational, reflection, and rotational semi-symmetries

## IV.A. Translations in 1D

Next let us consider a single degree of freedom system,  $x \in [-\pi, \pi]$ , in a potential energy landscape with n wells given by

$$U = a\cos(nx) - fx. (IV.1)$$

The potential energy, U, has translational symmetry when f=0. It is semi-symmetric when f is small enough. To be precise,  $U_{\mathcal{G}}(x) = a\cos(nx)$ ,  $\epsilon = f$ , and  $U_0(x) = -x$ . Let  $\tau_c$  be the translation operation by c such that  $\tau_c \cdot x = x + c$ . Then the symmetry of  $U_{\mathcal{G}}$  is described by the group

$$\mathcal{G} = \{ \dots, \tau_{-4\pi/n}, \tau_{-2\pi/n}, e, \tau_{2\pi/n}, \tau_{4\pi/n}, \dots \}.$$
 (IV.2)

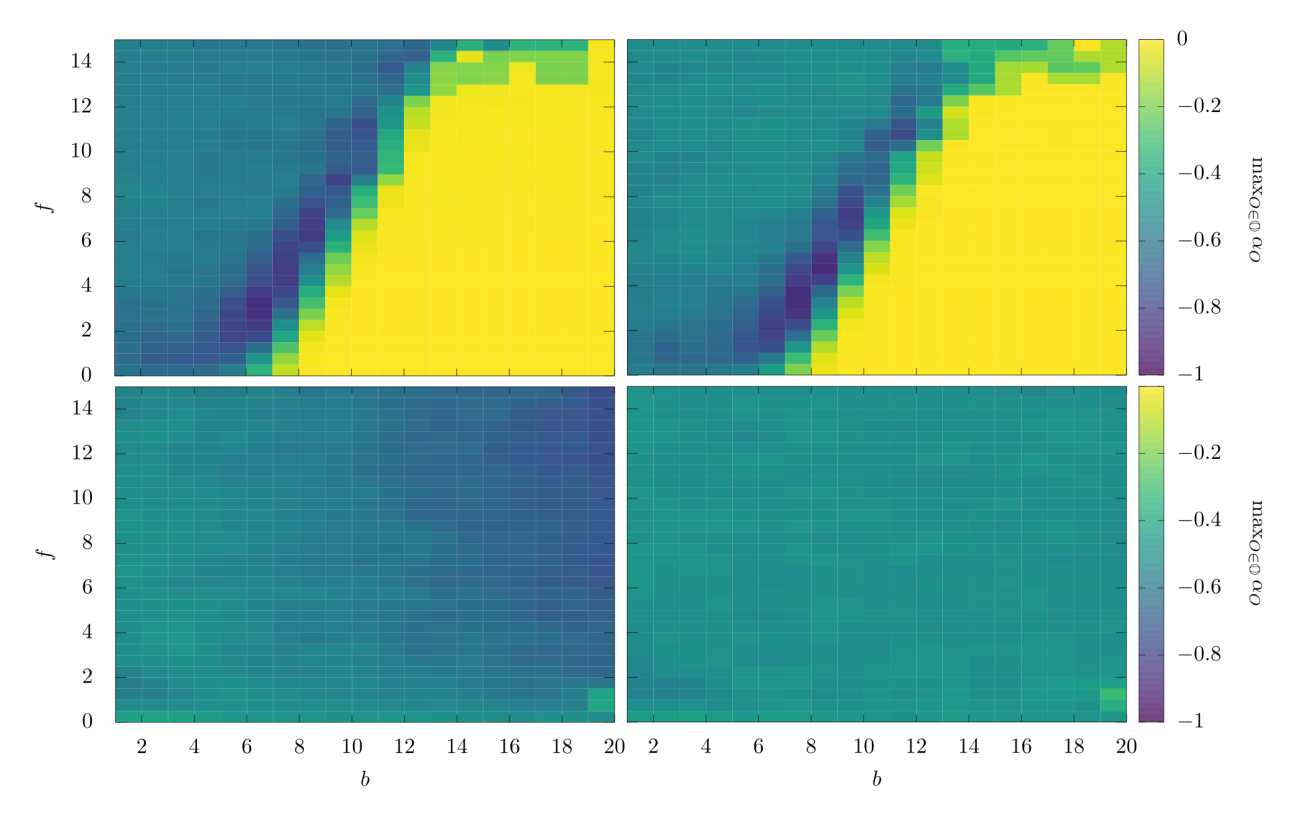
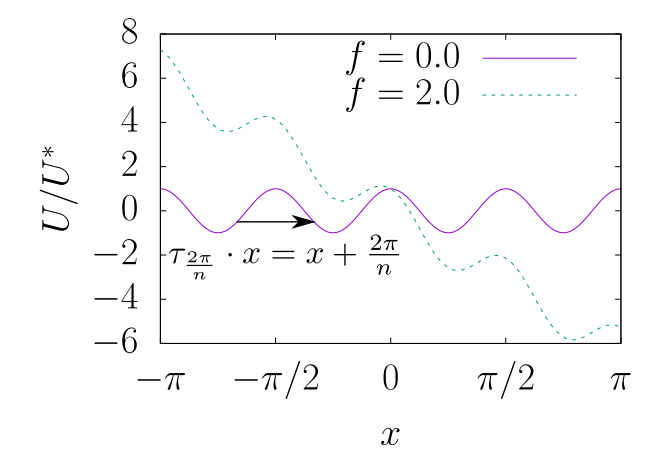


Figure 5: Convergence heat maps for double well potential. Heat maps of  $\max \alpha_O$ , which is a measure of the slowest convergence rate, as a function of b (x-axis) and f (y-axis) for the standard (top left), umbrella ( $\tilde{b}=4$ ) (top right), group-theoretic (bottom left), and group-theoretic with umbrella (bottom right) sampling approaches. For the non-group-theoretic approaches, the convergence rates dropoff quickly after a threshold in b-f space is crossed. While the umbrella sampling approach pushes this threshold to larger b (such that the method is robust for a larger region of parameter space), only the group-theoretic approaches show (sufficient) convergence for the entire parameter space.



Var.	Value
Γ	$ \begin{bmatrix} -\pi, \pi \\ a \cos(nx) \end{bmatrix} $
$U_{\mathcal{G}}$	$a\cos(nx)$
$\epsilon U_0$	-fx
${\cal G}$	$\left\{ \dots, \tau_{-4\pi/n}, \tau_{-2\pi/n}, e, \tau_{2\pi/n}, \tau_{4\pi/n}, \dots \right\}$
G	$ \begin{cases} -Jx \\ \{\dots, \tau_{-4\pi/n}, \tau_{-2\pi/n}, e, \tau_{2\pi/n}, \tau_{4\pi/n}, \dots\} \\ \{\tau_{-2\pi/n}, e, \tau_{2\pi/n}\} \\ 1/3 \text{ for all } i = 1, 2, 3 \end{cases} $
$\omega_i$	1/3 for all $i = 1, 2, 3$
$\ell^*$	$\begin{bmatrix} 2\pi/n \\ a \end{bmatrix}$
$U^*$	a
	l

Figure 6: Periodic potential and translation action. Potential energy given by  $U=a\cos{(nx)}-fx$  where a=1, and f=0 (solid line) and f=2 (dashed line). The potential energy has translational semi-symmetry; an example of one of its generating actions,  $\tau_{2\pi/n} \cdot x$ , is also shown.

Table 3: Properties of the translational semi-symmetric thermodynamic system and its associated group-theoretic sampling approach.

For our group-theoretic sampling, let us choose  $G = \{\tau_{-2\pi/n}, e, \tau_{2\pi/n}\}$  as our reversible generating set (i.e. the set contains the inverse of each of its elements) and sample each  $g \in G$  with probability 1/3. The energy landscape, its symmetry, and the effect of breaking symmetry (f > 0) are shown in figure 6 for a = 1 and n = 4. Examples of translational symmetries frequently occur in crystalline solids. Properties of the thermodynamic system and its associated group-theoretic sampling approach are summarized in table 3.

Table 4 shows the minimum convergence rate, maximum convergence rate, minimum error, and maximum error over  $\mathbb{O} = \{x, x^2, U, U^2\}$  as approximated using standard (denoted as 'SS'), umbrella ('US'), group-theoretic ('GT'), and group-theoretic & umbrella sampling ('GU'). For the umbrella sampling, Gaussian weights are fit to each of the energy barriers of  $U_{\mathcal{G}}$  such that the peak of each weight is centered at a peak of  $U_{\mathcal{G}}$ , the peak of each weight scales with a, and the width of each weight is fit to the width of each energy barrier. To be precise,

$$w(x) = a \sum_{i=1}^{N_w} \exp\left(\frac{-(x - x_i^0)^2}{2/n^2}\right),$$
 (IV.3)

where

$$\left\{x_i^0\right\}_{i=1}^{N_w} = \left\{\frac{2\pi m}{n} : m \in \mathbb{Z}, -\pi \le \frac{2\pi m}{n} \le \pi\right\}.$$
 (IV.4)

The first two examples (top left and top right) consist of  $\beta=10$  and energy landscapes with n=3 (which results in 4 energy wells) and a=1. The first (top left) has perfect translational symmetry since f=0; in the second (top right) example f=1. Here we see a phenomena similar to table 2. When f=0, the group-theoretic approaches show proper convergence rates while the non-group-theoretic approaches do not converge for all of the observables of interest (i.e.  $\max \alpha_O \geq 0$ ). When f=1 and symmetry is broken, the convergence rates of both the group-theoretic and non-group-theoretic approaches increase. The increase is such that some of the non-group-theoretic approaches converge more rapidly than their group-theoretic-based counterparts. However, it is noteworthy that the accuracy of the group-theoretic approaches are orders of magnitude greater than the non-group-theoretic approaches.

The last two examples (bottom left and bottom right) consist of  $\beta=10$ , and energy landscapes with n=5 (6 energy wells) and a=1. Similar phenomena can be observed regarding the f=0 (bottom left) and f=1 (bottom right) cases: the group-theoretic approaches consistently show rapid convergence and high accuracy. The non-group-theoretic approaches do not convergence for the f=0 case and are less accurate in general. Notice that the performance of the non-group-theoretic approaches is worse when there are more

	a=1, n	=3, f=0		$a = 1, n = 3, f = 1, \beta = 10.$					
method	$\min_{O \in \mathbb{O}} \alpha_O$	$\max_{O \in \mathbb{O}} \alpha_O$	$\min_{O\in\mathbb{O}}\mathcal{E}_O$	$\max_{O\in\mathbb{O}}\mathcal{E}_O$	method	$\min_{O \in \mathbb{O}} \alpha_O$	$\max_{O \in \mathbb{O}} \alpha_O$	$\min_{O\in\mathbb{O}}\mathcal{E}_O$	$\max_{O \in \mathbb{O}} \mathcal{E}_O$
SS	-0.5357	+0.0003	+0.0001	+0.6256	SS	-0.4973	-0.4933	+0.1768	+2.1221
US	-0.4649	+0.0269	+0.0001	+0.6261	US	-1.0548	-1.0502	+0.0049	+0.0592
GT	-0.5888	-0.4787	+0.0002	+0.0029	GT	-0.7084	-0.6523	+0.0001	+0.0023
GU	-0.5261	-0.4374	+0.0001	+0.0033	GU	-0.5050	-0.4901	+0.0001	+0.0020
	1					1			
	a=1, n	=5, f=0	), $\beta = 10$ .			a=1, n	=5, f=1	$1, \beta = 10.$	
method	$a = 1, n$ $\min_{O \in \mathbb{O}} \alpha_O$	$\frac{=5, f=0}{\max_{O\in\mathbb{O}}\alpha_O}$	$\frac{0, \ \beta = 10.}{\min_{O \in \mathbb{O}} \mathcal{E}_O}$	$\max_{O\in\mathbb{O}}\mathcal{E}_O$	method	$a = 1, n$ $\min_{O \in \mathbb{O}} \alpha_O$	$= 5, f = 1$ $\max_{O \in \mathbb{O}} \alpha_O$	$\frac{1, \ \beta = 10.}{\min_{O \in \mathbb{O}} \mathcal{E}_O}$	$\max_{O\in\mathbb{O}}\mathcal{E}_O$
method SS	$\min \alpha_O$	$\max \alpha_O$	$\min \mathcal{E}_{\mathcal{O}}$	$\max_{O \in \mathbb{O}} \mathcal{E}_O$ +1.9589	method SS	$\min \alpha_{O}$	$\max \alpha_O$	$\min \mathcal{E}_{O}$	$ \frac{\max_{O \in \mathbb{O}} \mathcal{E}_O}{+14.6097} $
	$\min_{O \in \mathbb{O}} \alpha_O$	$\max_{O \in \mathbb{O}} \alpha_O$	$\min_{O \in \mathbb{O}} \mathcal{E}_O$	<i>O</i> ∈0		$\min_{O \in \mathbb{O}} \alpha_O$	$\max_{O \in \mathbb{O}} \alpha_O$	$\min_{O \in \mathbb{O}} \mathcal{E}_O$	$O \in \mathbb{O}$
SS	$ \min_{O \in \mathbb{O}} \alpha_O \\ -0.5758 $	$\max_{O \in \mathbb{O}} \alpha_O +0.0002$	$ \min_{O \in \mathbb{O}} \mathcal{E}_O \\ +0.0001 $	$O \in \mathbb{O}$ +1.9589	SS	$ \min_{O \in \mathbb{O}} \alpha_O \\ -0.0108 $	$\max_{O \in \mathbb{O}} \alpha_O$ $-0.0054$	$ \min_{O \in \mathbb{O}} \mathcal{E}_O \\ +2.2519 $	$O \in \mathbb{O}$ +14.6097

Table 4: Error and convergence rates for periodic potential. Fastest rate of convergence,  $\min_{O \in \mathbb{O}} \alpha_O$ ; slowest rate of convergence,  $\max_{O \in \mathbb{O}} \alpha_O$ ; greatest accuracy,  $\min_{O \in \mathbb{O}} \mathcal{E}_O$ ; and least accuracy,  $\max_{O \in \mathbb{O}} \mathcal{E}_O$ , for each of the sampling approaches considered. The standard (denoted 'SS'), umbrella (denoted 'US'), group-theoretic (denoted 'GT') and group-theoretic with umbrella (denoted 'GU') sampling approaches are compared. Energy landscapes with various temperatures, barrier heights, a, number of local minima, n, and applied forces, f, are considered.

energy wells (i.e. n = 5) whereas performance of the group-theoretic approaches are consistent between n = 3 and n = 5. In summary, the group-theoretic approaches outperformed their counterparts for each of the examples considered; and the non-group-theoretic approaches were only viable options for one of the four examples considered (n = 3, f = 1).

Again, let us consider the interplay between two parameters of the system-well depth and the applied force—on the robustness of the various sampling approaches. Figure 7 shows heat maps of  $\max \alpha_O$  (i.e. slowest convergence rate over  $\mathbb{O}$ ) as a function of a (x-axis) and f (y-axis). Figure 7 compares the standard (top left), umbrella (top right), group-theoretic (bottom left), and group-theoretic & umbrella (bottom right) sampling approaches. For each case,  $\beta = 1$  and n = 4. There is a structure similar to that of figure 5. For the standard sampling approach (top left), there is a line, roughly 5+2.5a=f, that delineates two regions of convergence: the standard approach converges rapidly when 5 + 2.5a > f and does not convergence when 5 + 2.5a < f. Just to the left of the line,  $5+2.5a \gtrsim f$ , the convergence is at its most rapid. For the umbrella sampling approach, the convergence heat map is similar but shifted to the right such that convergence is achieved for a larger subregion of the parameter space (the line is roughly 7 + 2.5a = f, in this case). In contrast, the convergence rates of the group-theoretic approaches (bottom left and bottom right) are consistent throughout parameter space; the proposed method is shown to be robust for the energy landscapes considered. This may seem surprising initially, considering the underlying principle of the group-theoretic approach is to exploit symmetry and the parameter space considered is dense with asymmetric energy landscapes. To understand this, it helps to think of the group-theoretic approach as a kind of multiscale random walk which emulates diffusion at multiple scales. Through this lens it seems likely that, when simulating systems with broken symmetry, it is desirable for the generating set G to be small (or at least not too large). Indeed, consider figure 6: for  $f=2, x \to \tau_{\pm 2\pi/n} \cdot x$  results in a moderate change in energy but  $x \to \tau_{\pm 2\pi m/n} \cdot x$  for m>1results in a much greater change in energy. In this case, if the entire group of translational symmetries of  $U_{\mathcal{G}}$ were sampled, it would result in a larger proportion of rejections. Using a generating subset of  $\mathcal{G}$ , such as  $G = \{\tau_{-2\pi/n}, e, \tau_{2\pi/n}\}$ , as opposed to sampling  $\mathcal{G}$  itself, is analogous to sampling via the local jumps in the standard MCMC as opposed to sampling  $\Gamma$  directly. In either case, the more localized sampling approach takes advantage of the "smoothness" of the energy landscape in order to emphasize importance. The grouptheoretic approach allows one to make localized jumps where the notion of "localized" is generalized across multiple scales.

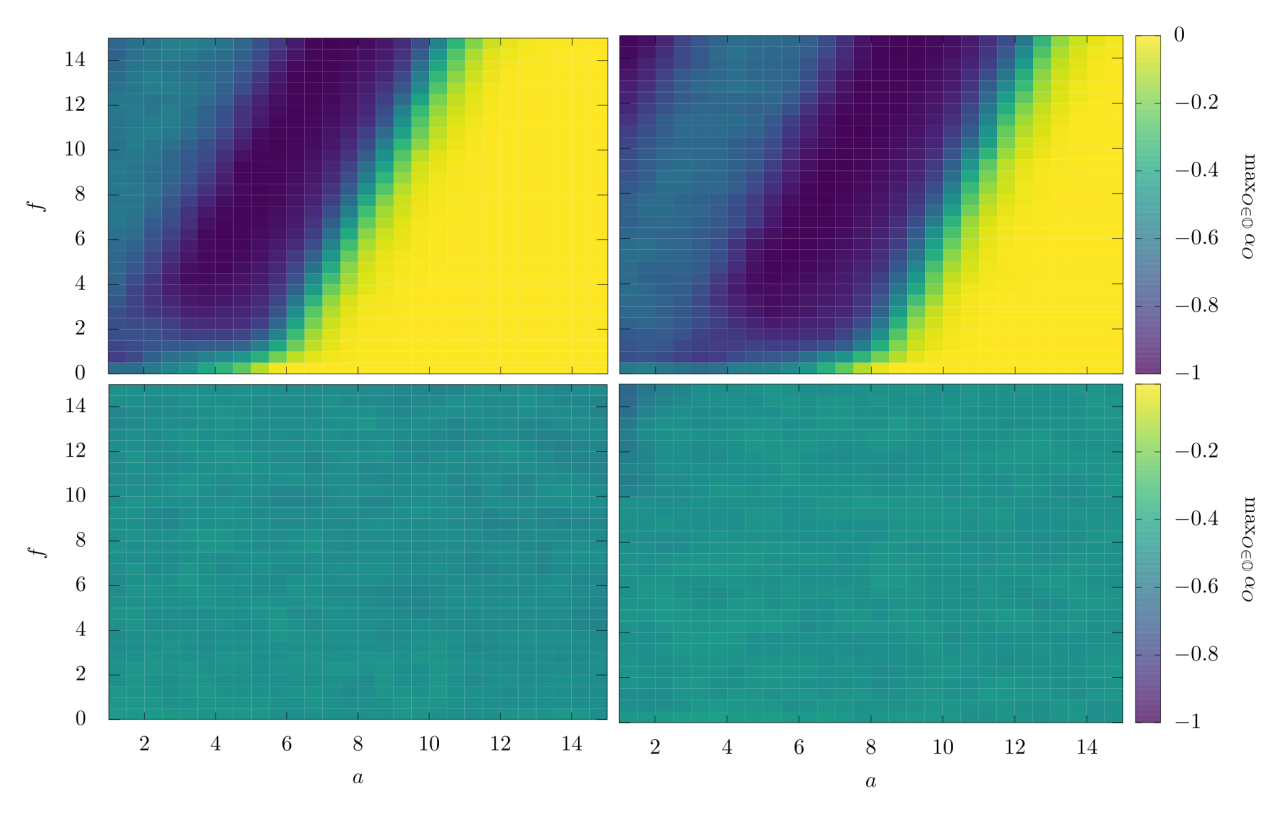


Figure 7: Convergence heat maps for periodic potential. Heat maps of  $\max \alpha_O$ , which is a measure of the slowest convergence rate, as a function of a (x-axis) and f (y-axis) for the standard (top left), umbrella (top right), group-theoretic (bottom left), and group-theoretic with umbrella (bottom right) sampling approaches. For each case,  $\beta=1$  and n=4. For the non-group-theoretic approaches, the convergence rates drop off quickly after a threshold in a-f space is crossed. While the umbrella sampling approach pushes this threshold to larger a (such that the method is robust for a larger region of parameter space), only the group-theoretic approaches show (sufficient) convergence for the entire parameter space.

#### IV.B. Octohedral, $\mathcal{D}_{4h}$ , and $\mathcal{D}_{2h}$ symmetries

Let us next consider a three degree of freedom system,  $\mathbf{x} \in [-\ell_1, \ell_1] \times [-\ell_2, \ell_2] \times [-\ell_3, \ell_3]$ , in an energy landscape given by

$$U = a \sum_{i=1}^{6} \phi(|\mathbf{x} - \mathbf{a}_i|) - \mathbf{f} \cdot \mathbf{x}$$
 (IV.5)

where

$$\mathbf{a}_{i} = \begin{cases} (\pm \ell_{1}, 0, 0) & i = 1, 2\\ (0, \pm \ell_{2}, 0) & i = 3, 4,\\ (0, 0, \pm \ell_{3}) & i = 5, 6 \end{cases}$$
 (IV.6)

and  $\phi$  is any pairwise potential which depends only on distance; and where boldface is used to emphasize that  $\mathbf{x}$ ,  $\mathbf{a}_i$ , and  $\mathbf{f}$  are all vectors. Note that the 'dot' operation in (IV.5) denotes the Euclidean inner product and not the application of a group action. Moving forward it should be clear from context which is meant as one is a binary operation between a group element and a vector and the other is a binary operation between pairs of vectors. The potential energy, U, has octohedral symmetry,  $\mathcal{O}_h$ , when  $f := |\mathbf{f}| = 0$  and  $\ell_1 = \ell_2 = \ell_3$ ,  $\mathcal{D}_{4h}$  symmetry (i.e. tetragonal symmetry) when  $\ell_1 = \ell_2 \neq \ell_3$  (or  $\ell_1 \neq \ell_2 = \ell_3$ , or  $\ell_1 = \ell_3 \neq \ell_2$ ), and  $\mathcal{D}_{2h}$  symmetry when  $\ell_1 \neq \ell_2 \neq \ell_3$ . It is semi-symmetric when f is small enough. Let  $\sigma_{\hat{\mathbf{u}}}$  be the reflection operation about the plane orthogonal to  $\hat{\mathbf{u}}$  such that  $\sigma_{\hat{\mathbf{u}}} \cdot \mathbf{x} = \mathbf{x} - 2(\hat{\mathbf{u}} \cdot \mathbf{x})\hat{\mathbf{u}}$ . For our group-theoretic sampling, let us choose  $G = \{e, \sigma_{\hat{\mathbf{e}}_1}, \sigma_{\hat{\mathbf{e}}_2}, \sigma_{\hat{\mathbf{e}}_3}\}$  as our generating set and sample each  $g \in G$  with probability 1/4. While G is a generating set of  $\mathcal{D}_{2h}$  but not  $\mathcal{D}_{4h}$  or  $\mathcal{O}_h$ , we will find that G is still sufficient for efficiently sampling the system regardless of which group describes  $U_{\mathcal{G}}$ . This is likely because  $\mathcal{D}_{2h} \leq \mathcal{D}_{4h} \leq \mathcal{O}_h^{-7}$  and G is sufficient for traversing energy barriers in any case. As a concrete example, let

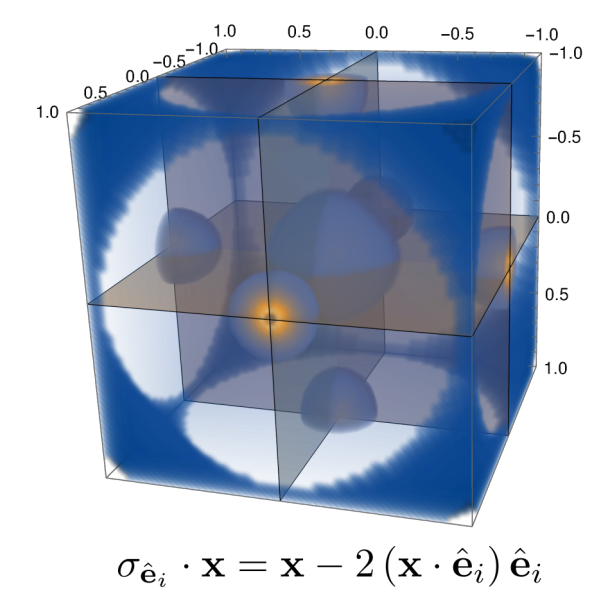
$$\phi\left(|\mathbf{x} - \mathbf{a}_i|\right) = |\mathbf{x} - \mathbf{a}_i|^{-1}.$$
 (IV.7)

The energy landscape for  $\ell_1 = \ell_2 = \ell_3 = 1$  and G are shown in figure 6. A physical example corresponding to this energy could result from an ionic particle diffusing through a lattice of (fixed) ions. A summary of the thermodynamic system and its group-theoretic properties is provided in table 5.

Figure 9 shows heat maps of the minimum convergence rate over  $\mathbb{O} = \{x_1, x_2, x_3, x_1^2, x_2^2, x_3^2, U, U^2\}$  as approximated using umbrella (top row) and group-theoretic (bottom row) sampling approaches for systems with different a and f. For the umbrella sampling,  $w(\mathbf{x}) = \exp\left(-|\mathbf{x}|^2/2\right)$ . The temperature is fixed such that  $\beta = 1$ . The left column corresponds to  $\hat{\mathbf{f}} = (1,0,0)$  and the right column corresponds to  $\hat{\mathbf{f}} = (1/\sqrt{3}, 1/\sqrt{3}, 1/\sqrt{3})$ . Notice that, for  $\hat{\mathbf{f}} = (1,0,0)$ , the convergence rate seems to be almost independent of f. Indeed, for the umbrella sampling approach, the convergence rate begins to drop off at a = 6 and vanishes when  $f \geq 10$ . For this case, the convergence of the group-theoretic approach is independent of f. This can be understood by considering the fact that the force, when directed toward  $\hat{\mathbf{f}} = (1,0,0)$ , only breaks the symmetry of the  $\sigma_{\hat{\mathbf{e}}_1}$  element. However, the (total) energy, U, is still invariant with respect to  $\sigma_{\hat{\mathbf{e}}_2}$  and  $\sigma_{\hat{\mathbf{e}}_3}$ . Alternatively, when  $\hat{\mathbf{f}} = \left(1/\sqrt{3}, 1/\sqrt{3}, 1/\sqrt{3}\right)$ , the umbrella sampling approach converges when f > a + 8. A key takeaway is that, when particles have more than one degree of freedom, both the magnitude and direction of  $\mathbf{f}$  relative to energy landscape are significant in determining whether or not a non-group-theoretic approaches can show proper convergence. While there is some variation of the convergence rate for the group-theoretic approach when  $\hat{\mathbf{f}} = \left(1/\sqrt{3}, 1/\sqrt{3}, 1/\sqrt{3}\right)$ , the method always convergences at a sufficient rate.

For completeness, let us also consider the maximum error over  $\mathbb{O}$  for the umbrella (left) and group-theoretic (right) methods when  $\hat{\mathbf{f}} = \left(1/\sqrt{3}, 1/\sqrt{3}, 1/\sqrt{3}\right)$ . Figure 10 shows that, although the convergence rates for umbrella sampling seem comparable to group-theoretic sampling for most of the parameter space considered in figure 9 (right column), there is a significant difference in the accuracy of the two approaches.

<sup>&</sup>lt;sup>7</sup>Whereby,  $\mathcal{H} \leq \mathcal{G}$ , it is meant that  $\mathcal{H}$  is a subgroup of  $\mathcal{G}$ .



Var. Value
$$\begin{array}{c|c}
\hline
\Gamma & [-\ell_1, \ell_1] \times [-\ell_2, \ell_2] \times [-\ell_3, \ell_3] \\
\hline
U_{\mathcal{G}} & a \sum_{i=1}^{6} |\mathbf{x} - \mathbf{a}_i| \\
\epsilon U_0 & -\mathbf{f} \cdot \mathbf{x} \\
\mathcal{G} & \mathcal{O}_h, \mathcal{D}_{4h}, \text{ or } \mathcal{D}_{2h} \\
G & \{e, \sigma_{\hat{\mathbf{e}}_1}, \sigma_{\hat{\mathbf{e}}_2}, \sigma_{\hat{\mathbf{e}}_3}\} \\
\omega_i & 1/4 \text{ for all } i = 1, \dots, 4 \\
\ell^* & \min \{\ell_1, \ell_2, \ell_3\} \\
U^* & a/\ell^*
\end{array}$$

Figure 8: Electrostatic potential from charges in a lattice and reflection actions. Potential energy given by  $U=a\sum_{i=1}^{6}|\mathbf{x}-\mathbf{a}_i|^{-1}-\mathbf{f}\cdot\mathbf{x}$  where  $a=1,\ell_1=\ell_2=\ell_3=1$  and f=0. The potential energy has reflection symmetries  $\sigma_{\hat{\mathbf{e}}_1},\sigma_{\hat{\mathbf{e}}_2}$ , and

Table 5: Properties of the multidimensional thermodynamic system with reflection and rotational semi-symmetries, and its associated group-theoretic sampling approach.

While each approach seems to have its lower accuracy for the a small and f large cases, the group-theoretic approach shows high accuracy for the remainder of parameter space. In contrast, the accuracy of the umbrella

#### IV.C. Summary and generalizations

sampling approach deteriorates as a increases.

 $\sigma_{\hat{\mathbf{e}}_3}$  (shown here via orange, opaque planes).

This work showed through example that the proposed approach, GA-MCMC, exhibits robust convergence rates and accuracy for a variety of systems and conditions (e.g. temperature, energy scales, length scales, etc.). The proposed approach was used for various types of discrete symmetries (e.g. translation, reflection, rotation) and for particles in both 1 dimension and 3 dimensions. Because, in each case, the dimensionality of  $\Gamma$  was small, it was feasible to compare the results of the MCMC simulations to integration by high-fidelity numerical quadrature. However, numerical experiments were also considered for which the number of particles were scaled up to tens or hundreds. The particles interacted through a short-range, hard-core potential; that is, if two particles were within r distance of each other, their interaction energy was considered infinite and vanished otherwise. While, in the interest of brevity, specific results are not discussed, I remark that the convergence and accuracy of the considered methods were similar to their previously discussed single particle counterparts provided  $r \ll \ell^*$  and the number of particles was not too large. In the next section, a many particle system with longer range interactions is considered. This will naturally lead to extending the principles developed in this section toward clustering-type algorithms.

An important consideration for the applicability of the group-theoretic approach is determining what discrete semi-symmetries are present and decomposing U into  $U_{\mathcal{G}}$  and  $\epsilon U_0$  accordingly. For this, the interested reader is referred to references on group theory and its application to physics: Hamermesh [46], Tinkham [81], Weyl [89].

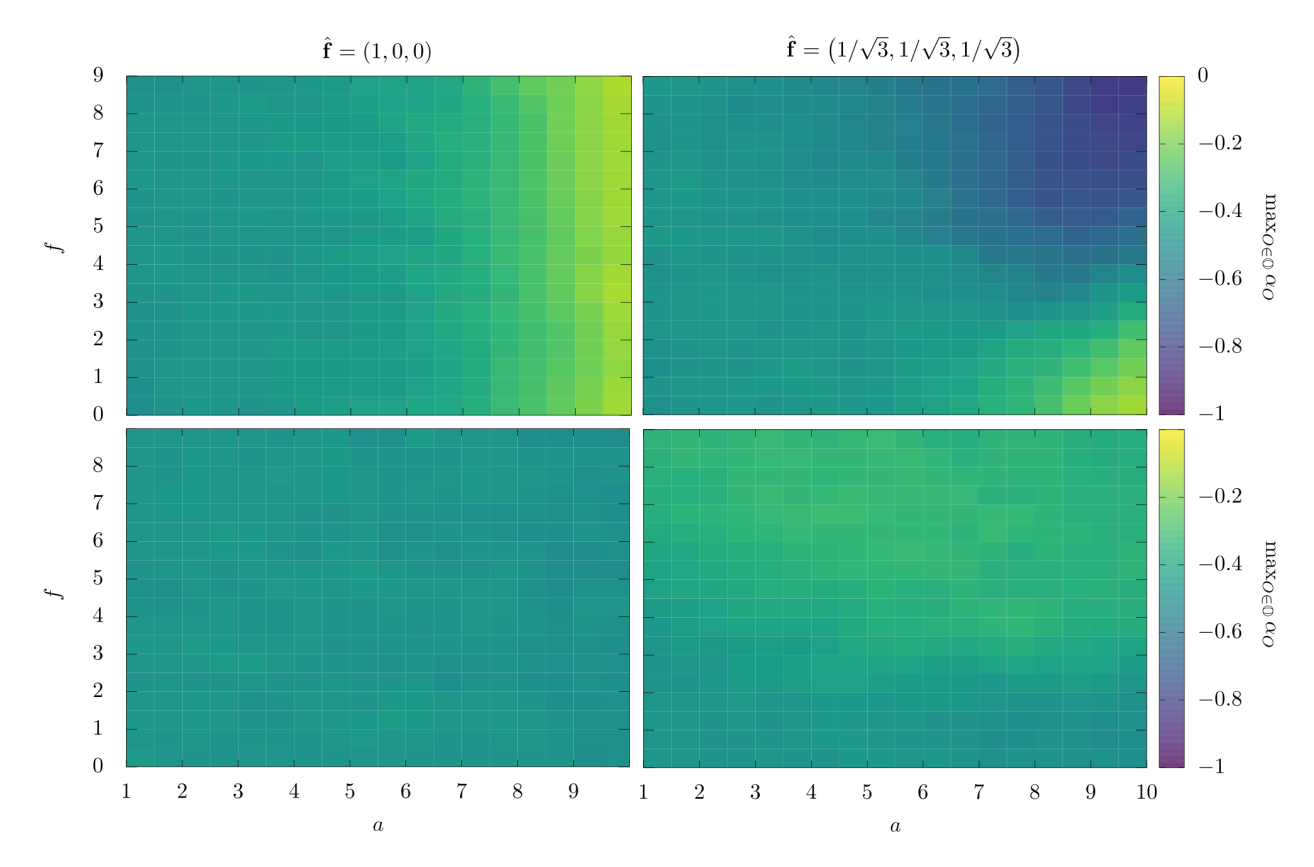


Figure 9: Convergence heat map for electrostatic potential from charges in a lattice. Heat maps of  $\max \alpha_O$ , which is a measure of the slowest convergence rate, as a function of a (x-axis) and f (y-axis) for the umbrella (top row), group-theoretic (bottom row) sampling approaches. The left column corresponds to  $\hat{\mathbf{f}}=(1,0,0)$  and the right column to  $\hat{\mathbf{f}}=\left(1/\sqrt{3},1/\sqrt{3},1/\sqrt{3}\right)$ . Notice that, increasing the magnitude of the applied force, f, only helps the umbrella approach with convergence in the  $\hat{\mathbf{f}}=\left(1/\sqrt{3},1/\sqrt{3},1/\sqrt{3}\right)$ ; this is because the components of the force need to be non-negligible in each of the  $\hat{\mathbf{e}}_1$ ,  $\hat{\mathbf{e}}_2$ , and  $\hat{\mathbf{e}}_3$  directions to break the discrete symmetries of the landscape. As expected, the group-theoretic has a sufficient convergence rate for the entire parameter space—regardless of  $\hat{\mathbf{f}}$ .

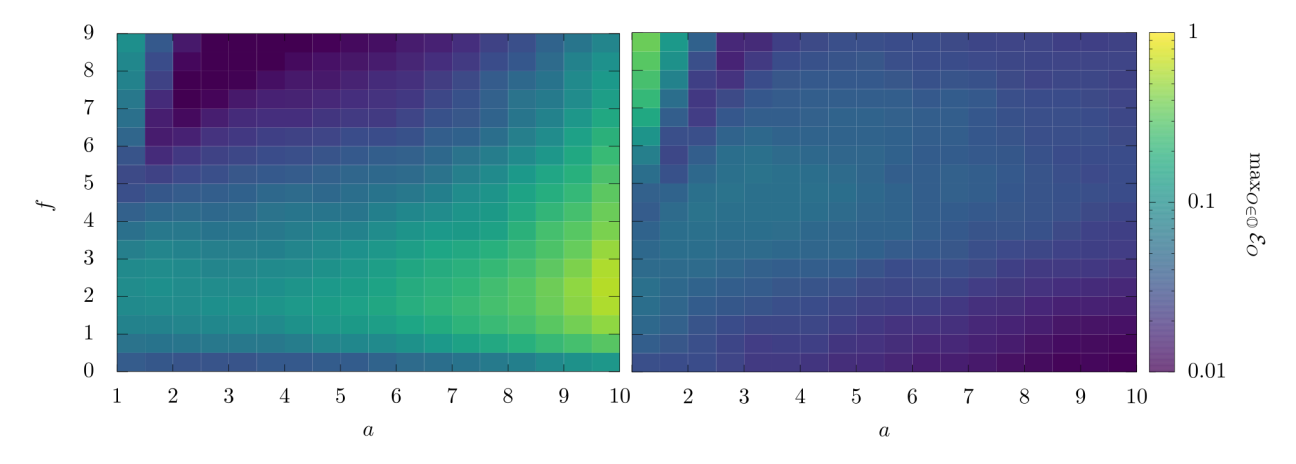


Figure 10: Error heat map for electrostatic potential from charges in a lattice. Maximum error over  $\mathbb O$  for the umbrella (left) and group-theoretic (right) methods when  $\hat{\mathbf f} = \left(1/\sqrt{3}, 1/\sqrt{3}, 1/\sqrt{3}\right)$ . While each approach seems to have its lower accuracy for the a small and f large cases, the group-theoretic approach shows high accuracy for the remainder of parameter space. In contrast, the accuracy of the umbrella sampling approach deteriorates as a increases.

## V. Dielectric polymers with monomer-monomer interactions

There has been a lot of interest in recent years in the mechanics of soft multifunctional materials; that is, soft materials which respond to external stimuli such as changes in ambient temperature, light, and/or electromagnetic fields [7, 8, 21–24, 37, 40, 41, 45, 60, 65, 67–69, 94]. Soft multifunctional materials are wellsuited for biologically inspired soft robotics, advanced prothestics, energy harvesting, energy absorption, and wearable sensors and electronics [49, 57, 60, 64, 67, 85]. For many of these applications, it is desirable to maximize the coupling between the external stimuli and mechanical deformation [7, 21, 67, 69]. To this end, statistical mechanics has proven useful for uncovering new types of couplings [22, 23, 43], new mechanisms for increasing couplings [44], and informing the design of materials with novel and enhanced properties [24, 39–41, 44]. Further, statistical mechanics may also play an important role in understanding the role of monomer-monomer interactions and possible associated phase transitions in soft multifunctional elastomers. If phase transitions occur under certain advantageous conditions, this could be leveraged as a means for increasing the magnitude or speed of response to external stimuli (e.g. phase transition enhanced actuation modes). However, when considering monomer-monomer interactions, obtaining an exact analytical solution(s) to the statistical mechanics formulation is often difficult, if not impossible [24, 31, 45, 73]; and, as we will encounter, there are difficulties inherent in simulating interacting polymer chains using MCMC as well. For dielectric elastomers—a class of soft materials which couple polarization and deformation to electric fields—many of the difficulties that occur when using standard MCMC methods are as a result of discrete symmetries and their associated energy barriers in the potential energy landscape [45]. This section will develop a group-theoretic sampling approach for dielectric polymer chains.

#### V.A. Statistical mechanics formulation

A polymer chain is a macro-molecule which consists of repeating units called monomers. While the shape of the polymer chain and the connectivity between monomers can take many different forms, let us restrict our attention to linear chains such that the monomers are bonded end-to-end. Besides the first and last monomers in a chain, each monomer has two neighbors to which it is bonded. (An example polymer chain is shown in figure 11.) Following a classical theory of polymer elasticity—the freely joint chain [86]—the mechanics of a polymer are idealized such that 1) monomers are rigid, 2) monomers are free to rotate about their neighboring bonds, and 3) excluded volume effects are neglected. This means the maximum length of the chain end-to-end vector (i.e. the vector which connects the beginning of the chain to its end),  $\mathbf{r}$ , is nb, where n is the number of monomers in the chain and b is the monomer length (i.e. Kuhn length). In this setting (e.g. linear chains with monomers of fixed length), the notion of the axis of a monomer is well-defined and the monomer's state is well described by the unit vector,  $\hat{\mathbf{n}}$ , along its axis which is oriented such that it points from the bond with its previous neighbor to the bond with its next neighbor. A microstate of the chain is then described by  $\mathbf{x} = (\hat{\mathbf{n}}_1, \dots, \hat{\mathbf{n}}_n)^{-8}$ . Here also,  $\Gamma = \mathbb{S}^2 \times \dots \times \mathbb{S}^2 = (\mathbb{S}^2)^n$ , and

$$\mathbf{r} = b \sum_{i=1}^{n} \hat{\mathbf{n}}_{i}. \tag{V.1}$$

Further, in the presence of an electric field, bound charges on a monomer can be separated to form an electric dipole,  $\mu$ . Given that the dipole depends on the magnitude of the electric field and the orientation of the monomer,  $\hat{\mathbf{n}}$ , relative to the direction of the electric field, it is standard to assume a simple anisotropic form [24, 78]:

$$\mu\left(\hat{\mathbf{n}}, \mathbf{E}_{0}\right) = \epsilon_{0} \chi_{\mu} \mathbf{E}_{0} = \epsilon_{0} \left[\chi_{\parallel} \hat{\mathbf{n}} \otimes \hat{\mathbf{n}} + \chi_{\perp} \left(\mathbf{I} - \hat{\mathbf{n}} \otimes \hat{\mathbf{n}}\right)\right] \mathbf{E}_{0} \tag{V.2}$$

where  $\chi_{\mu}$  is the dipole susceptibility tensor,  $\chi_{\parallel}$  and  $\chi_{\perp}$  are the dipole susceptibility along  $\hat{\bf n}$  and the susceptibility

$$\pi\left(\mathbf{x}\right)\propto\exp\left(-\beta U\left(\mathbf{x}\right)\right)\prod_{i=1}^{n}\sin\theta_{i},$$

where  $\theta_i$  is the polar angle of  $\hat{\mathbf{n}}_i$ .

<sup>&</sup>lt;sup>8</sup>Note that, when using spherical coordinates to describe  $(\mathbb{S}^2)^n$ , the unnormalized probability of a microstate must also include the Jacobian:

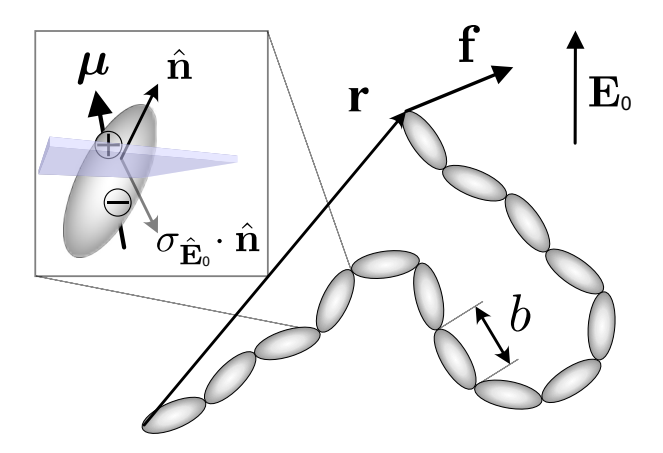


Figure 11: Freely jointed dielectric polymer chain with end-to-end vector,  $\mathbf{r}$ , applied force,  $\mathbf{f}$ , and applied electric field,  $\mathbf{E}_0$  (adapted with permission from [45]). Each monomer forms an electric dipole in response to the field and has a corresponding interaction energy. The monomer-field interaction energy has a discrete symmetry associated with the action  $\sigma_{\hat{\mathbf{E}}_0} \cdot \hat{\mathbf{n}}$  where  $\hat{\mathbf{n}}$  is the monomer direction (shown in upper left panel).

tibility in plane orthogonal to  $\hat{\mathbf{n}}$ , respectively,  $\mathbf{E}_0$  is the local electric field, and  $\epsilon_0$  is the vacuum permittivity. The electrostatic interaction of a single monomer with  $\mathbf{E}_0$  has two contributions: the energy associated with separating charges and the electric potential of a dipole in an electric field [40] <sup>9</sup>:

$$U_{E_0} = \frac{1}{2\epsilon_0} \boldsymbol{\mu} \cdot \boldsymbol{\chi}_{\mu}^{-1} \boldsymbol{\mu} - \boldsymbol{\mu} \cdot \mathbf{E}_0 = -\frac{1}{2} \boldsymbol{\mu} \cdot \mathbf{E}_0 = \frac{\epsilon_0 \Delta \chi}{2} \left( \mathbf{E}_0 \cdot \hat{\mathbf{n}} \right)^2 - \frac{\epsilon_0 \chi_{\perp}}{2} E_0^2, \tag{V.3}$$

where  $\Delta \chi = \chi_{\perp} - \chi_{\parallel}$ .

A constant force is applied to the end of the chain <sup>10</sup>. Given the models for the mechanical and dielectric responses of the monomers in the chain, we arrive at the energy for a dielectric polymer chain:

$$U = \sum_{i=1}^{n} \left( -\frac{1}{2} \boldsymbol{\mu}_i \cdot \mathbf{E}_0 \right) - \mathbf{f} \cdot \mathbf{r} - \sum_{i=1}^{n-1} \left( \frac{3 \left( \boldsymbol{\mu}_i \cdot \hat{\mathbf{q}}_{i,i+1} \right) \left( \boldsymbol{\mu}_{i+1} \cdot \hat{\mathbf{q}}_{i,i+1} \right) - \boldsymbol{\mu}_i \cdot \boldsymbol{\mu}_{i+1}}{4\pi \epsilon_0 q_{i,i+1}^3} \right)$$
(V.4)

where,  $\mathbf{q}_{i,j} = \mathbf{q}_i - \mathbf{q}_j$ ,  $q_{i,j} = |\mathbf{q}_{i,j}|$ ,  $\hat{\mathbf{q}}_{i,j} = \mathbf{q}_{i,j}/q_{i,j}$ ,

$$\mathbf{q}_{k} = \mathbf{q}_{k-1} + \frac{b}{2} \left( \hat{\mathbf{n}}_{k-1} + \hat{\mathbf{n}}_{k} \right) = b \sum_{i=1}^{k-1} \hat{\mathbf{n}}_{i} + \frac{b}{2} \hat{\mathbf{n}}_{k}; \text{ for } k = 2, \dots, n, \qquad \mathbf{q}_{1} = \frac{b}{2} \hat{\mathbf{n}}_{1}$$
 (V.5)

are the monomer positions, and  $\mathbf{f}$  is the applied force on the chain. The first term in (V.4) corresponds to the electrostatic interaction of the individual monomers with the applied field; the second term represents the work of the force done on the polymer chain; and the last term corresponds to the monomer-monomer interactions of induced dipoles within the monomers of the chain. For simplicity, the interaction energy only includes Ising-type nearest neighbor terms. See Grasinger and Dayal [40, 41], Grasinger et al. [45] for a more in-depth development of (V.2)-(V.5). Figure 11 shows a schematic of the system (adapted from [45]).

<sup>&</sup>lt;sup>9</sup>Where  $\chi_{\mu}^{-1}$  denotes the generalized inverse of  $\chi_{\mu}$ .

<sup>&</sup>lt;sup>10</sup>While, for simplicity, only the fixed force ensemble is considered, the principles developed herein would naturally extend to techniques used for efficiently sampling the fixed end-to-end vector ensemble such as the configurational-bias Monte Carlo [31, 72].

#### V.B. Semi-symmetries and energy barriers

Let  $\hat{\mathbf{E}}_0 = \mathbf{E}_0/E_0$ ,  $\mathbf{Q}_{\hat{\mathbf{E}}_0}(\varphi)$  denote a rotation about  $\hat{\mathbf{E}}_0$  by angle  $\varphi$ , and let  $\sigma_{\hat{\mathbf{E}}_0} = \mathbf{I} - 2\hat{\mathbf{E}}_0 \otimes \hat{\mathbf{E}}_0$  denote a reflection about the plane orthogonal to  $\hat{\mathbf{E}}_0$  where  $\otimes$  denotes the tensor product and  $\mathbf{I}$  is the identity tensor. It is easy to verify that 1)  $U_{E_0}\left(\mathbf{Q}_{\hat{\mathbf{E}}_0}(\varphi)\,\hat{\mathbf{n}}\right) = U_{E_0}\left(\hat{\mathbf{n}}\right)$  for all  $\varphi$  and  $\hat{\mathbf{n}}$ , and 2)  $U_{E_0}\left(\sigma_{\hat{\mathbf{E}}_0}\hat{\mathbf{n}}\right) = U_{E_0}\left(\hat{\mathbf{n}}\right)$  for all  $\hat{\mathbf{n}}$ . The symmetry of '1)' is a continuous symmetry and does not have any energy barriers associated with it; therefore standard MCMC trial moves (e.g. standard jumps, hybrid Monte Carlo, etc.) are sufficient for sampling this symmetry. However, '2)', is a discrete symmetry. For dielectric polymer chains where  $\chi_{\parallel} > \chi_{\perp}$ ,  $\hat{\mathbf{E}}_0 \cdot \hat{\mathbf{n}} = 0$  is an energy barrier which separates wells at  $\hat{\mathbf{E}}_0 \cdot \hat{\mathbf{n}} = \pm 1$ . When  $\beta \epsilon_0 E_0^2 \chi_{\parallel}/2$  is large enough, standard MCMC methods suffer from a poor convergence rate because each monomer in the chain becomes localized at one of the two wells and cannot readily pass through  $\hat{\mathbf{E}}_0 \cdot \hat{\mathbf{n}} = 0$  to the other well [45].

Given the results of previous sections, we may consider letting  $G = \{e, \sigma_{\hat{\mathbf{E}}_0}\}$  and augmenting the standard MCMC trial move by sampling and applying an action from G. To be precise, we may randomly choose some  $i \in \{1, \ldots, n\}$ , perturb  $\hat{\mathbf{n}}_i$ , and then  $\hat{\mathbf{n}}_i \to g_j \cdot \hat{\mathbf{n}}_i$  where  $g_j \in G$  are sampled via the weights  $\omega_1 = \omega_2 = 1/2$ . This sampling algorithm was shown to improve convergence in [45] for dielectric chains in which monomermonomer interactions are negligible. In this work, however, there are additional considerations related to monomer-monomer interactions.

Consider the Ising-type (nearest neighbor) monomer-monomer interaction term in (V.4). First, isolate a single contribution to the sum: the interaction between neighbors i and i+1. It will now be shown that this interaction term is invariant with respect to simultaneous reflection of monomers i and i+1; that is, the action  $\hat{\mathbf{n}}_i \to \sigma_{\hat{\mathbf{E}}_0} \hat{\mathbf{n}}_i$  and  $\hat{\mathbf{n}}_{i+1} \to \sigma_{\hat{\mathbf{E}}_0} \hat{\mathbf{n}}_{i+1}$ . Upon application of the action  $\hat{\mathbf{n}}_i \to \sigma_{\hat{\mathbf{E}}_0} \hat{\mathbf{n}}_i$ , the dipole at monomer i takes the form (see (V.2)):

$$\boldsymbol{\mu}_{i} \to \epsilon_{0} \Delta \chi \left( \mathbf{E}_{0} \cdot \sigma_{\hat{\mathbf{E}}_{0}} \hat{\mathbf{n}}_{i} \right) \sigma_{\hat{\mathbf{E}}_{0}} \hat{\mathbf{n}}_{i} + \epsilon_{0} \chi_{\perp} \mathbf{E}_{0} = -\sigma_{\hat{\mathbf{E}}_{0}} \boldsymbol{\mu}_{i}$$
 (V.6)

such that, when  $\hat{\mathbf{n}}_i \to \sigma_{\hat{\mathbf{E}}_0} \hat{\mathbf{n}}_i$  and  $\hat{\mathbf{n}}_{i+1} \to \sigma_{\hat{\mathbf{E}}_0} \hat{\mathbf{n}}_{i+1}$  are applied simultaneously, the inner product  $\boldsymbol{\mu}_i \cdot \boldsymbol{\mu}_{i+1}$  remains unchanged. Similarly, by (V.5)

$$\mathbf{q}_{i,i+1} = \frac{b}{2} \left( \hat{\mathbf{n}}_i + \hat{\mathbf{n}}_{i+1} \right) \to \frac{b}{2} \left( \sigma_{\hat{\mathbf{E}}_0} \hat{\mathbf{n}}_i + \sigma_{\hat{\mathbf{E}}_0} \hat{\mathbf{n}}_{i+1} \right) = \sigma_{\hat{\mathbf{E}}_0} \mathbf{q}_{i,i+1}$$
 (V.7)

upon simultaneous reflection of i and i+1. Thus, both quantities:  $q_{i,i+1}$  and

$$(\boldsymbol{\mu}_i \cdot \hat{\mathbf{q}}_{i,i+1}) (\boldsymbol{\mu}_{i+1} \cdot \hat{\mathbf{q}}_{i,i+1}) \tag{V.8}$$

are invariant with respect to the simultaneous reflection of monomers i and i+1 (i.e.  $\hat{\mathbf{n}}_i \to \sigma_{\hat{\mathbf{E}}_0} \hat{\mathbf{n}}_i$  and  $\hat{\mathbf{n}}_{i+1} \to \sigma_{\hat{\mathbf{E}}_0} \hat{\mathbf{n}}_{i+1}$ ); and, hence, the interaction energy between monomers i and i+1 is also invariant.

The above analysis elucidates more about the discrete semi-symmetries of (V.4). Several remarks are in order:

- 1) While the interaction energy between monomers i and i + 1 is invariant with respect to simultaneous reflection, the interaction energy can vary greatly when a monomer is reflected but one of its neighbors is not.
- 2) In general, the interaction energy between monomers i and i+1 is at a minimum when  $\hat{\mathbf{n}}_i = \hat{\mathbf{n}}_{i+1}$  and diverges when  $\hat{\mathbf{n}}_i = -\hat{\mathbf{n}}_{i+1}$ .
- 3) A straightforward way of decomposing U into  $U_{\mathcal{G}} + \epsilon U_0$  would be

$$U_{\mathcal{G}} := \sum_{i=1}^{n} \left( -\frac{1}{2} \boldsymbol{\mu}_{i} \cdot \mathbf{E}_{0} \right) - \sum_{i=1}^{n-1} \left( \frac{3 \left( \boldsymbol{\mu}_{i} \cdot \hat{\mathbf{q}}_{i,i+1} \right) \left( \boldsymbol{\mu}_{i+1} \cdot \hat{\mathbf{q}}_{i,i+1} \right) - \boldsymbol{\mu}_{i} \cdot \boldsymbol{\mu}_{i+1}}{4\pi \epsilon_{0} q_{i,i+1}^{3}} \right). \tag{V.9}$$

$$\epsilon U_{0} := -\mathbf{f} \cdot \mathbf{r}$$

Here  $\mathcal{G} = \{e, \Sigma\}$  where  $\Sigma \cdot \mathbf{x} = \left(\sigma_{\hat{\mathbf{E}}_0} \hat{\mathbf{n}}_1, \dots, \sigma_{\hat{\mathbf{E}}_0} \hat{\mathbf{n}}_n\right)$ . The issue with taking  $G = \mathcal{G}$  is two-fold: a)

application of  $\Sigma$  causes a significant change in  $\mathbf{r}$  as  $\mathbf{r} \to \sigma_{\hat{\mathbf{E}}_0} \mathbf{r}$ , and, consequently, a significant change in the work of the applied force; and b) the orbit of  $\langle \langle G \rangle \rangle$  will not contain many additional microstates in  $\Gamma$  (in fact, it, at most, contains two distinct elements whereas there are significantly more than two local minima in  $\Gamma$ ).

By remark 1, it is, in some way, suboptimal to merely augment the standard MCMC jumps by reflecting a single monomer about the plane orthogonal to  $\hat{\mathbf{E}}_0$ . By remark 3, it is also suboptimal to merely augment the standard jumps by simultaneously reflecting all of the monomers in the chain. This naturally leads us to the idea of clustering (see [80, 90], §5.2.3 of [53], and §14 of [31] for example).

#### V.C. Group-theoretic clustering of dielectric polymers

Here GA-MCMC is generalized for the clustering of dielectric polymer chains, and systems with interacting particles and discrete symmetries—more broadly. The basic idea is to randomly construct a variable sized cluster of neighboring monomers in the polymer chain and reflect them simultaneously. Because clusters are generally constructed to be larger than a single monomer, this effectively transitions the microstate between disparate energy wells. Because the cluster is of variable size, its successive action samples a greater number of distinct microstates. Both properties enhance the overall mixing of the chain.

To be precise, let us randomly choose some monomer, k. Then we add monomer k+1 to the cluster with probability,  $\zeta_{k,k+1}$ . If monomer k+1 was added to the cluster, we continue by adding its next neighbor k+2, and so on, again with probability  $\zeta_{k+1,k+2}$ , until either the trial expansion of the cluster has been rejected or we have reached the end of the chain. Upon completion, let us expand the cluster in the opposite direction, starting with k-1, then k-2, and so on, until either a trial expansion has been rejected or we have reached the beginning of the chain. We then sample  $G = \{e, \sigma_{\hat{\mathbf{E}}_0}\}$ , each element with a probability 1/2, and apply its action to each monomer in the cluster.

Two details remain: 1) specification of  $\zeta_{(\cdot,\cdot)}$  and 2) determination of the Hastings factor,  $\mathcal{H}(\mathbf{y} \to \mathbf{x})$  (see (I.7)). Beginning with '2)', we consider  $t(\mathbf{x} \to \mathbf{y})$ . Assume for now that the  $\zeta_{i,j}$  are symmetric with respect to transposition of its indices, i.e.  $\zeta_{i,j} = \zeta_{j,i}$ . Let the cluster span from monomer r to monomer s. Then

$$t(\mathbf{x} \to \mathbf{y}) = \frac{1}{2} t_{\text{in}} (1 - \zeta_{r-1,r}) \zeta_{r,r+1} \zeta_{r+1,r+2} \dots \zeta_{s-1,s} (1 - \zeta_{s,s+1}),$$
 (V.10)

where 1/2 is the probability of sampling either e or  $\sigma_{\hat{\mathbf{E}}_0}$  from G,  $t_{\rm in}$  is the probability of beginning the construction of the cluster by randomly choosing some monomer within it,  $(1-\zeta_{r-1,r})$  is the probability of not adding monomer r-1 to the cluster,  $\zeta_{r,r+1}$  is the probability of expanding the cluster from r to r+1 (or vice versa), etc <sup>11</sup>. The probability  $t(\mathbf{x} \to \mathbf{y})$  is simply the product over the probabilities of each of the individual events which make up the trial proposition because they are mutually independent events. Given  $(\mathbf{V}.10)$ , the Hastings factor is

$$\mathcal{H}(\mathbf{y} \to \mathbf{x}) = \frac{\left(1 - \zeta'_{m-1,m}\right) \zeta'_{m,m+1} \zeta'_{m+1,m+2} \dots \zeta'_{n-1,n} \left(1 - \zeta'_{n,n+1}\right)}{\left(1 - \zeta_{m-1,m}\right) \zeta_{m,m+1} \zeta_{m+1,m+2} \dots \zeta_{n-1,n} \left(1 - \zeta_{n,n+1}\right)},$$
(V.11)

where  $\zeta_{i,j}$  and  $\zeta'_{i,j}$  are the cluster expansion probabilities for the forward and reverse trial moves, respectively (i.e.  $\mathbf{x} \to \mathbf{y}$  and  $\mathbf{y} \to \mathbf{x}$ , respectively); and where the  $t_{\rm in}$  factors cancel because  $t_{\rm in}$  is independent of the current state and only depends on the cluster size (which is the same for both the forward and reverse moves). For convenience, efficiency, and in the interest of keeping the Hastings factor as close to 1 as possible, it is desirable that  $\zeta_{i,j} = \zeta'_{i,j}$  for as many i and j as possible. This, together with remark 1 and 2, leads naturally to the following construction: let

$$\zeta_{i,j} = \zeta \left( \hat{\mathbf{n}}_i \cdot \hat{\mathbf{n}}_j, \left( \hat{\mathbf{n}}_i \cdot \hat{\mathbf{E}}_0 \right)^2, \left( \hat{\mathbf{n}}_j \cdot \hat{\mathbf{E}}_0 \right)^2, \dots; \beta, \mathbf{E}_0, \chi_{\parallel}, \chi_{\perp}, b, n, \dots \right); \tag{V.12}$$

<sup>&</sup>lt;sup>11</sup>Here the condition  $\zeta_{i,j} = \zeta_{j,i}$  simplifies the calculation considerably. Because the probability is the same whether the cluster is expanding in increasing index (i.e. from r to r + 1) or decreasing index (i.e. from r + 1 to r), we do not need to explicitly consider the monomer at which the cluster started.

that is, let  $\zeta_{i,j}$  be a function of the state variables of the polymer chain and other properties of the thermodynamic system which are invariant with respect to the action  $\hat{\mathbf{n}}_i \to \sigma_{\hat{\mathbf{E}}_0} \hat{\mathbf{n}}_i$  and  $\hat{\mathbf{n}}_j \to \sigma_{\hat{\mathbf{E}}_0} \hat{\mathbf{n}}_j$ . In this case, (V.11) simplifies to

$$\mathcal{H}\left(\mathbf{y} \to \mathbf{x}\right) = \frac{\left(1 - \zeta_{m-1,m}'\right) \left(1 - \zeta_{n,n+1}'\right)}{\left(1 - \zeta_{m-1,m}\right) \left(1 - \zeta_{n,n+1}\right)},\tag{V.13}$$

Here, again motivated by remark 1 and 2, the simple choice of

$$\zeta_{i,j} = \begin{cases} \zeta\left(\hat{\mathbf{n}}_i \cdot \hat{\mathbf{n}}_j\right) = \frac{1 + \hat{\mathbf{n}}_i \cdot \hat{\mathbf{n}}_j}{2} & 1 \le i \le n, 1 \le j \le n \\ 0 & \text{otherwise} \end{cases}$$
(V.14)

is made; as it has the property that, if  $\hat{\mathbf{n}}_i = \hat{\mathbf{n}}_j$ —which is energetically favorable—monomer i and j are always clustered together and, consequently, will continue to be aligned after the reflection action on the cluster. Whereas, when  $\hat{\mathbf{n}}_i = -\hat{\mathbf{n}}_j$ , which is energetically unfavorable, monomer i and j are never clustered together and, consequently,  $\hat{\mathbf{n}}_i \neq -\hat{\mathbf{n}}_j$  after the reflection action on the cluster (except in the special case of  $\hat{\mathbf{n}}_c \cdot \hat{\mathbf{E}}_0 = 0$  where c equals whichever of the two monomers, i or j, is contained in the cluster). It is likely that more sophisticated forms of (V.12) which include information about the temperature, electric field, etc., could be constructed to have better convergence properties than (V.14); this is a potential topic for future work. However, it will be shown that, for the examples considered herein, (V.14) performs well.

#### V.D. Verification and results

The group-theoretic clustering algorithm for dielectric polymers is briefly verified here. For the special case of when monomer-monomer interactions are negligible and  $\mathbf{f}/f = \pm \mathbf{E}_0$ , an exact solution to the statistical mechanics formulation is possible (see [45] §5.3 for more detail). To verify the proposed approach, the interaction term in the MCMC simulations is (temporarily) dropped and its results are compared with the exact solution. Of particular interest in dielectric polymers, is the polymer chain elasticity; that is, its response to the applied force, f. Let  $\lambda = r/nb$  denote the (absolute) stretch of the polymer chain. Then the response  $\lambda = \lambda(\mathbf{f}, \dots)$  also depends on the temperature, electric field, dielectric properties, and other state variables of the polymer chain. Let us restrict our attention to polymer chains with  $\chi_{\parallel}>0$  and  $\chi_{\perp} = 0$  throughout the remainder of the work-since the energy barrier (induced by the discrete symmetry of the electric field interaction) only occurs when  $\chi_{\parallel} > \chi_{\perp}$ . In this case, it is energetically favorable for monomers to align with the axis of the electric field (i.e.  $\hat{\mathbf{n}} = \pm \mathbf{E}_0$ ). Thus, the polymer chains become less stiff (i.e. the polymer chain stretches more for the same magnitude of applied force) when stretched in ±E<sub>0</sub> [23, 24, 39–41, 43]. Figure 12 compares the predicted stretch response for dielectric polymer chains where interactions are negligible and the force is applied in the electric field direction. The temperature and dielectric properties are constant at  $\beta = 1$ ,  $\epsilon_0 = 1$ , and  $\chi_{\parallel} = 1$ , respectively. All simulations were run for  $10^6$ steps. Figure 12.a compares the exact solution to MCMC simulations using standard ('SS') and umbrella ('US') sampling. While the predictions are nearly exact for  $E_0 = 0$ , the agreement is poor for  $E_0 = 5$ ; there is significant noise in the predictions for  $f \leq 1$ . This is because monomers in the chain become localized to either  $\hat{\mathbf{n}} = \pm \hat{\mathbf{E}}_0$  and cannot traverse the energy barrier at  $\hat{\mathbf{n}} \cdot \hat{\mathbf{E}}_0 = 0$ . Figure 12.b compares the exact solution to MCMC simulations using the group-theoretic clustering approach for  $E_0 = 0, 1, 2, 3$ , and 5. The predictions and corresponding exact solutions are shown to agree well.

Having verified the group-theoretic clustering approach, let us next consider the effects of monomer-monomer interactions on the convergence properties of the MCMC approaches and the physics of dielectric polymer chains. An analytical solution (exact or approximate) is not readily obtainable in this case and because it involves high-dimensional integration, we cannot readily compare the MCMC predictions to high-fidelity numerical quadrature. As a result, the definitions and calculations for  $\alpha_O$  and  $\mathcal{E}_O$  are adjusted slightly. Here 25 different MCMC simulations are run for  $\mathcal{K}=10^6$  steps and for each of the sampling approaches. For the remainder of this section, let  $\alpha_O$  be calculated by fitting a line (using least squares) to the  $\log |\overline{\langle O \rangle_K} - \overline{\langle O \rangle_K}|$  vs.  $\log K$  data where  $\overline{\square}$  denotes the sample average (over MCMC simulations) of  $\square$  and K is the step number. The measure of convergence rate,  $\alpha_O$ , is taken to be the slope of this line.

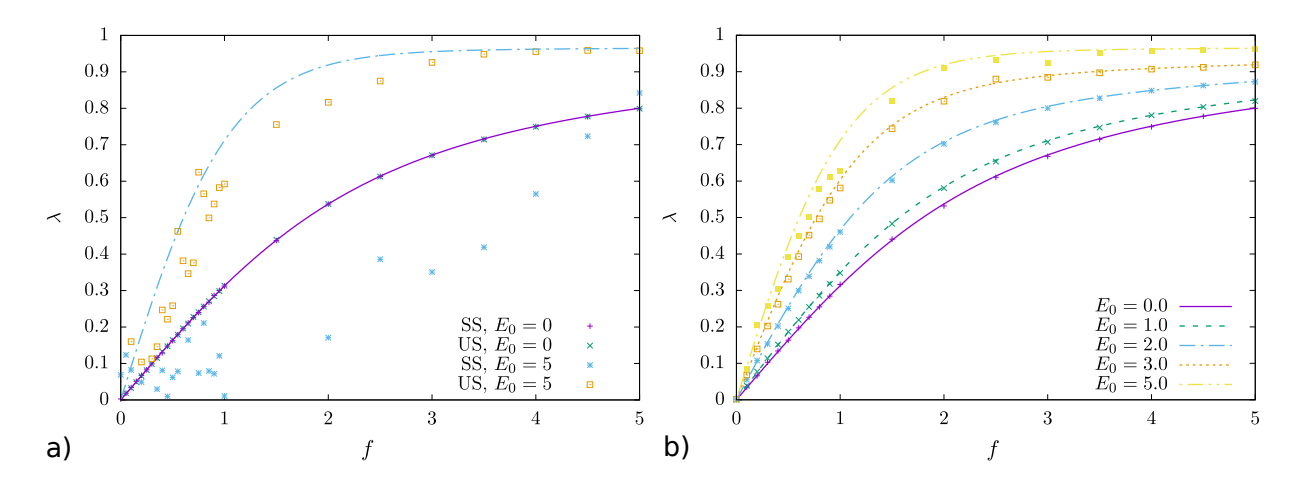


Figure 12: Electroelasticity of a dielectric polymer chain with non-interacting monomers. Force-stretch curves for dielectric polymer chains with  $\beta=1$  and  $\chi_{\parallel}=1$ , and non-interacting monomers. a) compares the exact solution to MCMC simulations using standard ('SS') and umbrella ('US') sampling. While the predictions are nearly exact for  $E_0=0$ , the agreement is poor for  $E_0=5$ . This is because monomers in the chain become localized to either  $\hat{\bf n}=\pm\hat{\bf E}_0$  and cannot traverse the energy barrier at  $\hat{\bf n}\cdot\hat{\bf E}_0=0$ . b) compares the exact solution to MCMC simulations using the group-theoretic clustering approach for  $E_0=0,1,2,3$ , and 5. The predictions and corresponding exact solutions are shown to agree well.

Similarly,

$$\mathcal{E}_O := \frac{1}{O^*} \left( \overline{\left| \langle O \rangle_{\mathcal{K}} - \overline{\langle O \rangle_{\mathcal{K}}} \right|} \right). \tag{V.15}$$

Next let

$$\mathbf{p} = \sum_{i=1}^{n} \mu_i \tag{V.16}$$

denote the net dipole of the polymer chain. Then

$$\mathbb{O} = \left\{ r_1, r_2, r_3, p_1, p_2, p_3, U, r_1^2, r_2^2, r_3^2, p_1^2, p_2^2, p_3^2, U^2 \right\}, \tag{V.17}$$

$$r^* = b, p^* = \epsilon_0 \chi_{\parallel} E_0, \text{ and } U^* = \chi_{\parallel} E_0^2.$$

In the interest of completeness, the convergence rate and accuracy is compared for the standard ('SS'), umbrella ('US'), and group-theoretic ('GT') sampling approaches for various dielectric polymer chains in table 6. For each example, n=100,  $\epsilon_0=1$ ,  $\chi_{\parallel}=1$ , and b=1. Let the coordinate system be Euclidean and such that  $\hat{\mathbf{e}}_3=\hat{\mathbf{E}}_0$ ; then  $f_1=\mathbf{f}\cdot\hat{\mathbf{e}}_1$  and  $f_3=\mathbf{f}\cdot\hat{\mathbf{e}}_3$  are the components of the force in the direction orthogonal to  $\hat{\mathbf{E}}_0$  and in the direction of  $\hat{\mathbf{E}}_0$ , respectively. The performance of each of the sampling approaches are compared for different electric field magnitudes, force components in the  $\hat{\mathbf{e}}_1$  and  $\hat{\mathbf{e}}_3$  direction, and temperatures. As expected, the group-theoretic clustering algorithm is the only approach to consistently perform well in all of the cases considered. In contrast, the non-group-theoretic approaches are only viable when the applied force has appropriate direction and magnitude to break symmetry sufficiently.

Before closing, we consider the effect of monomer-monomer interactions on the elasticity of dielectric polymer chains. The polymer chain stretch,  $\lambda$ , as a function of f is shown in figure 13. Similar to figure 12: n=100, b=1,  $\beta=1$ ,  $\epsilon_0=1$ ,  $\chi_{\parallel}=1$ , and the force is applied to the polymer chain such that  $\mathbf{f}/f=\hat{\mathbf{E}}_0$ . Here the MCMC simulations (depicted with markers, denoted by 'GT') include the energy of monomer-monomer interactions. The MCMC simulations are compared with the exact results of the non-interacting dielectric chain (depicted by lines, denoted by 'NI'); however, in this case the comparison is not made to assess the fit of the MCMC simulations. Instead, the comparison is made in order to isolate the effect of monomer-monomer interactions on the elasticity of the polymer chains. The force-stretch curves are shown for  $E_0=1$  (green 'x' markers and dashed line),  $E_0=2$  (blue '\* markers and dot-dashed line), and  $E_0=3$  (orange ' $\Box$ ' markers and dashed line). In every case, the MCMC simulations predict a polymer chain which is less stiff (i.e. stretches more at equal applied force) than its non-interacting counterpart.

$E_0 = 1, f_1 = 0, f_3 = 0, \beta = 1.$					$E_0 = 1, f_1 = 0, f_3 = 0, \beta = 10.$				
method	$\lim_{O\in\mathbb{O}}\alpha_O$	$\max_{O \in \mathbb{O}} \alpha_O$	$\min_{O\in\mathbb{O}}\mathcal{E}_O$	$\max_{O \in \mathbb{O}} \mathcal{E}_O$	method	$\min_{O \in \mathbb{O}} \alpha_O$	$\max_{O \in \mathbb{O}} \alpha_O$	$\min_{O\in\mathbb{O}}\mathcal{E}_O$	$\max_{O \in \mathbb{O}} \mathcal{E}_O$
SS	-0.9940	-0.3702	+0.0298	+0.7868	SS	-0.8177	+0.1826	+0.0690	
US	-0.2196	6 - 0.0884	+0.9429	+269.58	US	-0.0017	+0.0006	+2.2442	+515578
GT	-0.5170	-0.2227	+0.0531	+0.8753	GT	-0.8383	-0.2059	+0.0879	+5.2789
	,					,			
1	$E_0 = 1, f_1$	$=0, f_3=$	$1, \beta = 10.$			$E_0 = 1, f$	$f_1 = 1, f_3$	$=0, \beta=1$	0.
method	$\min_{O \in \mathbb{O}} \alpha_O$	$\max_{O \in \mathbb{O}} \alpha_O$	$\min_{O \in \mathbb{O}} \mathcal{E}_O$	$\max_{O \in \mathbb{O}} \mathcal{E}_O$	method	$\min_{O \in \mathbb{O}} \alpha_O$	$\max_{O \in \mathbb{O}} \alpha_O$	$\min_{O \in \mathbb{O}} \mathcal{E}_O$	$\max_{O \in \mathbb{O}} \mathcal{E}_O$
SS	-1.4812	-0.5055	+0.0163	+1.5976	SS	-0.9514	-0.3526	+0.1285	+0.8324
US	-0.5297	-0.1147	+0.0727	+0.1510	US	-0.0000	+0.0000	+1.9725	+1717.2384
$\operatorname{GT}$	-1.3466	-0.5288	+0.0146	+0.2882	$\operatorname{GT}$	-1.0133	-0.4446	+0.1042	+0.9607
					,				
	$E_0 = 5,$	$f_1 = 0, f_3$	$=0, \ \beta=1$			$E_0 = 3, j$	$f_1 = 3, f_3$	$=3, \beta=1$	
method	$ \min_{O \in \mathbb{O}} \alpha_O $	$\max_{O \in \mathbb{O}} \alpha_O$	$\min_{O \in \mathbb{O}} \mathcal{E}_O$	$\max_{O \in \mathbb{O}} \mathcal{E}_O$	method	$\min_{O \in \mathbb{O}} \alpha_O$	$\max_{O \in \mathbb{O}} \alpha_O$	$\min_{O \in \mathbb{O}} \mathcal{E}_O$	$\max_{O \in \mathbb{O}} \mathcal{E}_O$
SS	-0.6788	+0.0723	+0.0546	+21.403	SS	-1.4082	-0.7502	+0.0398	+0.1001
US	-0.0000	+0.0000	+1.6537	+1101.6	US	-0.7065	-0.4341	+0.0580	+0.1551
GT	-1.2398	-0.4721	+0.0179	+1.4278	GT	-1.1827	-0.4405	+0.0324	+0.1500

Table 6: Error and convergence rates for dielectric polymer chain (with monomer-monomer interactions). Fastest rate of convergence,  $\min_{O \in \mathbb{O}} \alpha_O$ ; slowest rate of convergence,  $\max_{O \in \mathbb{O}} \alpha_O$ ; greatest accuracy,  $\min_{O \in \mathbb{O}} \mathcal{E}_O$ ; and least accuracy,  $\max_{O \in \mathbb{O}} \mathcal{E}_O$ , for each of the sampling approaches considered. The standard (denoted 'SS'), umbrella (denoted 'US'), and group-theoretic (denoted 'GT') are compared. Dielectric polymer chains with various  $E_0$ ,  $f_1$  (component of force orthogonal to field direction),  $f_3$  (component of force in the field direction), and  $\beta$  are shown. The group-theoretic clustering algorithm is the only approach to consistently perform well in all of the cases considered

This can be understood as follows: regarding monomer-monomer interactions, it is energetically favorable (i.e. the interaction energy is at its minimum) for neighboring monomers to be aligned (i.e.  $\hat{\mathbf{n}}_i = \hat{\mathbf{n}}_{i+1}$ ); and the interaction energy diverges as the neighboring monomers have opposite directions (i.e.  $\hat{\mathbf{n}}_i \to -\hat{\mathbf{n}}_{i+1}$ ). Recall figure 12.b. The interaction of the individual monomers with the electric field causes monomers in the polymer chain to prefer to align along the axis of the electric field direction,  $\hat{\mathbf{n}}_i = \pm \hat{\mathbf{E}}_0$ . Since the elasticity of polymer chains is driven by entropy, the preferred alignment along  $\pm \mathbf{E}_0$  results in the polymer chain being less stiff (i.e. more compliant) when stretched in the  $\pm \ddot{\mathbf{E}}_0$  directions. The solutions for the noninteracting system ('NI') shown in figure 13 isolate this effect. When the energy of interactions is included (see 'GT' curves) there are two main contributions to the decrease in stiffness in the  $\pm \mathbf{E}_0$  directions: 1) the electric field interaction, again, causes monomers to align in the  $\pm \hat{\mathbf{E}}_0$  directions and 2) monomers also prefer to align with their neighbors. The second contribution serves to amplify the first. Thus, we see that, when the energy of monomer-monomer interactions is included in the statistical mechanics treatment, it results in the prediction of decreased stiffness in the  $\mathbf{E}_0$  direction. Interestingly, there is nearly a discontinuous jump in  $\lambda$  about  $f \gtrsim 0$  for the case of  $E_0 = 3$ . While speculative, this may signify the potential onset of a phase transition in the polymer chain for some combination of finite  $E_0, \chi_{\parallel}, n, b$  and  $\beta$ . An in-depth study of the statistical physics of dielectric polymer chains with monomer-monomer interactions—with an emphasis on phase transitions and the efficacy of exploiting phase transitions for novel electromechanical properties—will be studied in future work.

This section highlights the utility of GA-MCMC for simulating more practical, interacting, and high-dimensional thermodynamic systems. The statistical mechanics formulation for many multifunctional elastomers have a similar structure: there are field-monomer and monomer-monomer interactions which include even powers of  $\hat{\bf n}$  and the applied force term which is linear in  $\hat{\bf n}$  (e.g. liquid crystal elastomers [26]). In such cases, a clustering-type GA-MCMC with inversion actions  $(\hat{\bf n} \to -\hat{\bf n})$  or reflection about special planes (e.g. field-induced) may pose a promising approach.

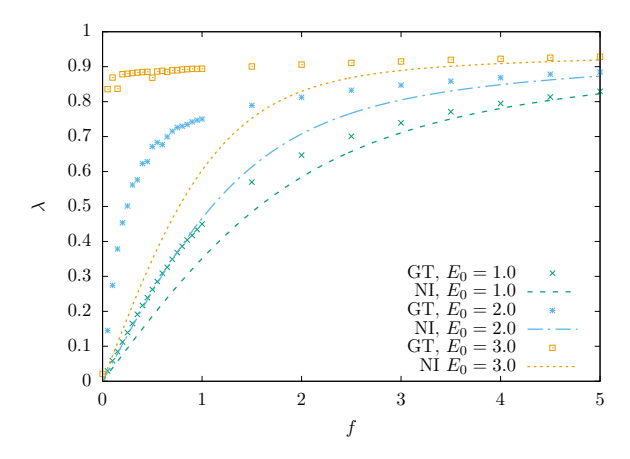


Figure 13: Electroelasticity of a dielectric polymer chain with monomer-monomer interactions. Force-stretch curves for dielectric polymer chains with  $\beta=1$  and  $\chi_{\parallel}=1$ , and monomer-monomer interactions. To isolate the effect of monomer-monomer interactions, the predictions made which include monomer-monomer interactions (denoted by 'GT') are shown in comparison with the non-interacting solutions (denoted by 'NI'). The force-stretch curves are shown for  $E_0=1$  (green 'x' markers and dashed line),  $E_0=2$  (blue '\*' markers and dot-dashed line), and  $E_0=3$  (orange ' $\Box$ ' markers and dashed line). When the energy of monomer-monomer interactions is included in the statistical mechanics treatment, it results in the prediction of decreased stiffness in the  $\hat{\bf E}_0$  direction; in other words, the polymer chain stretches more in response to an equal amount of applied force. Interestingly, there is nearly a discontinuous jump in  $\lambda$  about  $f \gtrsim 0$  for the case of  $E_0=3$ —which may indicated the onset of a phase transition.

## VI. Conclusion

Summary and contributions. When significant contributions to the potential energy of a thermodynamic system have discrete symmetries, it can lead to energy landscapes with multiple local minima separated by large energy barriers. A sampling approach (GA-MCMC) was proposed which, in addition to standard jumps, randomly applies group actions from a generating set(s) of the group(s) which describes the discrete symmetries. It was shown through both simple, low-dimensional examples (section III and IV), and a more practical, complex, and high-dimensional example—an interacting dielectric polymer chain—that the proposed approach is consistently more efficient and robust than some of the more popular alternatives for energy landscapes with large barriers (e.g. umbrella sampling). Past work has suggested (albeit informally) the potential advantages of making "symmetry jumps" [34] between modes in a multimodal probability distribution. However, to this author's knowledge, this is the first work to 1) propose decomposing the potential energy function (or functional) into a part with discrete symmetries,  $U_{\mathcal{G}}$ , and an asymmetric part,  $\epsilon U_0$ , 2) formalize the idea of "symmetric jumps" in the language of group theory, and 3) propose sampling from a generating set(s) to efficiently propagate between energy wells (i.e. modes of the distribution).

Outlook: Machine learning of discrete symmetries and adaptive GA-MCMC. A limitation of the proposed approach is that it requires U in explicit form and some insight into an appropriate decomposition of  $U = U_{\mathcal{G}} + \epsilon U_0$ . Toward this end, there is an extensive body of work on understanding the symmetries of various energy functions (and functionals) and microstructures of interest because of its utility in quantum mechanics [9, 46, 66, 81, 89], crystalline lattices [46, 48, 81], martensitic phase transitions [16, 17], nanostructures [25, 36, 48, 92]—as well as many other applications. If little is known about U, however, one may have to resort to other means. A potential path forward may be to use replica exchange and machine learning to develop an adaptive GA-MCMC. To be more specific, let  $D: \theta \times \Gamma \mapsto \Gamma$  be an operator which depends on parameter(s)  $\theta$  and (for fixed  $\theta$ ) maps  $\Gamma$  to itself. Then one can imagine learning discrete (semi-)symmetry operators by finding local minimizers of

$$\theta^* = \arg\min_{\theta} \left\{ \left( \int_{\Gamma} dx \left| U\left(D\left(\theta, x\right)\right) - U\left(x\right) \right| \right) + \kappa \left\| D - e \right\| \right\}$$
 (VI.1)

where the second term penalizes operators that are too close to the identity operator, e,  $\|.\|$  is an appropriate operator norm, and  $\kappa$  is the weight of the penalty. There are two main difficulties with (VI.1): 1) it is not

obvious how to enforce that D is a discrete symmetry, and 2) the integral in (VI.1) is again, of course, high-dimensional. Replica exchange MCMC is a kind of brute force sampling approach which can be used at the outset of the simulation when there is little to no information about U in order to perform the required integration. As more and more samples are taken, (VI.1) can be solved to greater accuracy. One can then choose some m (discrete) local minimizers of (VI.1),  $\tilde{D}_i = D|_{\theta=\theta_i^*}$ , and let  $G = \left\{\tilde{D}_1^{-1}, \ldots, \tilde{D}_m^{-1}, e, \tilde{D}_1, \ldots, \tilde{D}_m\right\}$  where the weights can even be scaled such that they are lesser for greater loss and vice versa. Machine learning methods have been used to successfully learn operators for partial differential equations [15, 52, 95] and may generalize to (VI.1) or similar loss functions. The recent work Bronstein et al. [19] may also relevant as it considers symmetry, invariance, and equivariance in the context of deep learning. The current work suggests that such an adaptive procedure, though expensive, could be lead to greater efficiency for energy landscapes with discrete symmetries and even be the difference between converging or not converging (in a reasonable number of steps). As mentioned previously, despite not being strictly memoryless, the adaptive "Markov" chain is still guaranteed to converge to the underlying probability distribution asymptotically provided the adaption procedure vanishes asymptotically [20].

## Software availability

All of the research code written for this work is open source. A version of the code used to generate the results of sections III and IV can be found at https://github.com/grasingerm/polya-mcmc. A version of the code used for simulating dielectric polymer chains in section V can be found at https://github.com/grasingerm/polymer-stats.

## Acknowledgments

The author acknowledges computation resources provided by the Extreme Science and Engineering Discovery Environment (XSEDE) [84], which is supported by National Science Foundation grant number ACI-1548562. The author also acknowledges insightful discussions and encouragement towards pursuit of the topic from Kaushik Dayal, Pradeep Sharma, Prashant Purohit, Aziz Fall, Shoham Sen, and Kosar Mozaffari.

#### References

- [1] Elena Akhmatskaya, Nawaf Bou-Rabee, and Sebastian Reich. A comparison of generalized hybrid monte carlo methods with and without momentum flip. *Journal of Computational Physics*, 228(6):2256–2265, 2009.
- [2] Michael P Allen and Dominic J Tildesley. Computer simulation of liquids. Oxford university press, 2017.
- [3] Joshua A Anderson, Eric Jankowski, Thomas L Grubb, Michael Engel, and Sharon C Glotzer. Massively parallel monte carlo for many-particle simulations on gpus. *Journal of Computational Physics*, 254:27– 38, 2013.
- [4] Christophe Andrieu, Nando De Freitas, Arnaud Doucet, and Michael I Jordan. An introduction to mcmc for machine learning. *Machine learning*, 50(1):5–43, 2003.
- [5] Yves F Atchadé and Jeffrey S Rosenthal. On adaptive markov chain monte carlo algorithms. Bernoulli, 11(5):815–828, 2005.
- [6] Yves F Atchadé, Gareth O Roberts, and Jeffrey S Rosenthal. Towards optimal scaling of metropoliscoupled markov chain monte carlo. Statistics and Computing, 21(4):555–568, 2011.
- [7] Mahnoush Babaei, Junfeng Gao, Arul Clement, Kaushik Dayal, and M Ravi Shankar. Torque-dense photomechanical actuation. *Soft Matter*, 17(5):1258–1266, 2021.
- [8] Ruobing Bai and Kaushik Bhattacharya. Photomechanical coupling in photoactive nematic elastomers. Journal of the Mechanics and Physics of Solids, 144:104115, 2020.

- [9] Amartya S Banerjee. Ab initio framework for systems with helical symmetry: theory, numerical implementation and applications to torsional deformations in nanostructures. *Journal of the Mechanics and Physics of Solids*, page 104515, 2021.
- [10] Christian Bartels and Martin Karplus. Probability distributions for complex systems: adaptive umbrella sampling of the potential energy. *The Journal of Physical Chemistry B*, 102(5):865–880, 1998.
- [11] Jarle Berntsen, Terje O Espelid, and Alan Genz. An adaptive algorithm for the approximate calculation of multiple integrals. ACM Transactions on Mathematical Software (TOMS), 17(4):437–451, 1991.
- [12] Alexandros Beskos, Natesh Pillai, Gareth Roberts, Jesus-Maria Sanz-Serna, and Andrew Stuart. Optimal tuning of the hybrid monte carlo algorithm. *Bernoulli*, 19(5A):1501–1534, 2013.
- [13] Michael Betancourt. Identifying the optimal integration time in hamiltonian monte carlo. arXiv preprint arXiv:1601.00225, 2016.
- [14] Michael Betancourt. A conceptual introduction to hamiltonian monte carlo. arXiv preprint arXiv:1701.02434, 2017.
- [15] Saakaar Bhatnagar, Yaser Afshar, Shaowu Pan, Karthik Duraisamy, and Shailendra Kaushik. Prediction of aerodynamic flow fields using convolutional neural networks. *Computational Mechanics*, 64(2):525– 545, 2019.
- [16] Kaushik Bhattacharya. Microstructure of martensite: why it forms and how it gives rise to the shape-memory effect, volume 2. Oxford University Press, 2003.
- [17] Kaushik Bhattacharya, Sergio Conti, Giovanni Zanzotto, and Johannes Zimmer. Crystal symmetry and the reversibility of martensitic transformations. *Nature*, 428(6978):55–59, 2004.
- [18] William M Bolstad. Understanding computational Bayesian statistics, volume 644. John Wiley & Sons, 2009.
- [19] Michael M Bronstein, Joan Bruna, Taco Cohen, and Petar Veličković. Geometric deep learning: Grids, groups, graphs, geodesics, and gauges. arXiv preprint arXiv:2104.13478, 2021.
- [20] Steve Brooks, Andrew Gelman, Galin Jones, and Xiao-Li Meng. *Handbook of markov chain monte carlo*. CRC press, 2011.
- [21] Lingling Chen, Xu Yang, Binglei Wang, Shengyou Yang, Kaushik Dayal, and Pradeep Sharma. The interplay between symmetry-breaking and symmetry-preserving bifurcations in soft dielectric films and the emergence of giant electro-actuation. *Extreme Mechanics Letters*, 43:101151, 2021.
- [22] Noy Cohen. A generalized electro-elastic theory of polymer networks. Journal of the Mechanics and Physics of Solids, 110:173–191, 2018.
- [23] Noy Cohen and Gal deBotton. Electromechanical interplay in deformable dielectric elastomer networks. *Physical review letters*, 116(20):208303, 2016.
- [24] Noy Cohen, Kaushik Dayal, and Gal deBotton. Electroelasticity of polymer networks. *Journal of the Mechanics and Physics of Solids*, 92:105–126, 2016.
- [25] Kaushik Dayal and Richard D James. Nonequilibrium molecular dynamics for bulk materials and nanostructures. *Journal of the Mechanics and Physics of Solids*, 58(2):145–163, 2010.
- [26] Pierre-Gilles De Gennes and Jacques Prost. *The physics of liquid crystals*. Number 83. Oxford university press, 1993.
- [27] Christophe Dress and Werner Krauth. Cluster algorithm for hard spheres and related systems. *Journal of Physics A: Mathematical and General*, 28(23):L597, 1995.

- [28] Simon Duane, Anthony D Kennedy, Brian J Pendleton, and Duncan Roweth. Hybrid monte carlo. *Physics letters B*, 195(2):216–222, 1987.
- [29] Traian Dumitrică and Richard D James. Objective molecular dynamics. *Journal of the Mechanics and Physics of Solids*, 55(10):2206–2236, 2007.
- [30] Michael Engel, Joshua A Anderson, Sharon C Glotzer, Masaharu Isobe, Etienne P Bernard, and Werner Krauth. Hard-disk equation of state: First-order liquid-hexatic transition in two dimensions with three simulation methods. *Physical Review E*, 87(4):042134, 2013.
- [31] Daan Frenkel and Berend Smit. Understanding molecular simulation: from algorithms to applications, volume 1. Elsevier, 2001.
- [32] Dani Gamerman and Hedibert F Lopes. Markov chain Monte Carlo: stochastic simulation for Bayesian inference. CRC Press, 2006.
- [33] Andrew Gelman, Gareth O Roberts, and Walter R Gilks. Efficient metropolis jumping rules. *Bayesian statistics*, 5(599-608):42, 1996.
- [34] Charles J Geyer. Markov chain monte carlo maximum likelihood. 1991.
- [35] Charles J Geyer and Elizabeth A Thompson. Annealing markov chain monte carlo with applications to ancestral inference. *Journal of the American Statistical Association*, 90(431):909–920, 1995.
- [36] Swarnava Ghosh, Amartya S Banerjee, and Phanish Suryanarayana. Symmetry-adapted real-space density functional theory for cylindrical geometries: Application to large group-iv nanotubes. *Physical Review B*, 100(12):125143, 2019.
- [37] Andrea Giudici and John S Biggins. Large deformation analysis of spontaneous twist and contraction in nematic elastomer fibers with helical director. *Journal of Applied Physics*, 129(15):154701, 2021.
- [38] Sharon C Glotzer and Wolfgang Paul. Molecular and mesoscale simulation methods for polymer materials. *Annual Review of Materials Research*, 32(1):401–436, 2002.
- [39] Matthew Grasinger. Multiscale Modeling and Theoretical Design of Dielectric Elastomers. PhD thesis, Carnegie Mellon University, 2019.
- [40] Matthew Grasinger and Kaushik Dayal. Statistical mechanical analysis of the electromechanical coupling in an electrically-responsive polymer chain. *Soft Matter*, 16:6265–6284, 2020.
- [41] Matthew Grasinger and Kaushik Dayal. Architected elastomer networks for optimal electromechanical response. *Journal of the Mechanics and Physics of Solids*, 146:104171, 2021. ISSN 0022-5096.
- [42] Matthew Grasinger, Daniel O'Malley, Velimir Vesselinov, and Satish Karra. Decision analysis for robust co2 injection: application of bayesian-information-gap decision theory. *International Journal of Greenhouse Gas Control*, 49:73–80, 2016.
- [43] Matthew Grasinger, Carmel Majidi, and Kaushik Dayal. Nonlinear statistical mechanics drives intrinsic electrostriction and volumetric torque in polymer networks. *Physical Review E*, 103:042504, 2021.
- [44] Matthew Grasinger, Kosar Mozaffari, and Pradeep Sharma. Flexoelectricity in soft elastomers and the molecular mechanisms underpinning the design and emergence of giant flexoelectricity. *Proceedings of the National Academy of Sciences*, 118(21), 2021. ISSN 0027-8424.
- [45] Matthew Grasinger, Kaushik Dayal, Gal deBotton, and Prashant K. Purohit. Statistical mechanics of a dielectric polymer chain in the force ensemble. *Journal of the Mechanics and Physics of Solids*, 158: 104658, 2022. ISSN 0022-5096.
- [46] Morton Hamermesh. Group theory and its application to physical problems. Courier Corporation, 2012.

- [47] JR Heringa and HWJ Blöte. Geometric cluster monte carlo simulation. *Physical Review E*, 57(5):4976, 1998.
- [48] Richard D James. Objective structures. Journal of the Mechanics and Physics of Solids, 54(11):2354–2390, 2006.
- [49] Seung-Yeol Jeon, Beijun Shen, Nicholas A Traugutt, Zeyu Zhu, Lichen Fang, Christopher M Yakacki, Thao D Nguyen, and Sung Hoon Kang. Synergistic energy absorption mechanisms of architected liquid crystal elastomers. arXiv preprint arXiv:2110.07461, 2021.
- [50] Johannes Kästner. Umbrella sampling. Wiley Interdisciplinary Reviews: Computational Molecular Science, 1(6):932–942, 2011.
- [51] Aaron S Keys and Sharon C Glotzer. How do quasicrystals grow? *Physical Review Letters*, 99(23): 235503, 2007.
- [52] Nikola Kovachki, Zongyi Li, Burigede Liu, Kamyar Azizzadenesheli, Kaushik Bhattacharya, Andrew Stuart, and Anima Anandkumar. Neural operator: Learning maps between function spaces. arXiv preprint arXiv:2108.08481, 2021.
- [53] Werner Krauth. Statistical mechanics: algorithms and computations, volume 13. Oxford University Press, 2006.
- [54] Shankar Kumar, John M Rosenberg, Djamal Bouzida, Robert H Swendsen, and Peter A Kollman. The weighted histogram analysis method for free-energy calculations on biomolecules. i. the method. *Journal* of computational chemistry, 13(8):1011–1021, 1992.
- [55] Shiwei Lan, Tan Bui-Thanh, Mike Christie, and Mark Girolami. Emulation of higher-order tensors in manifold monte carlo methods for bayesian inverse problems. *Journal of Computational Physics*, 308: 81–101, 2016.
- [56] David Landau and Kurt Binder. A guide to Monte Carlo simulations in statistical physics. Cambridge university press, 2021.
- [57] Jing Li, Lichen Fang, Bohan Sun, Xixing Li, and Sung Hoon Kang. Recent progress in flexible and stretchable piezoresistive sensors and their applications. *Journal of The Electrochemical Society*, 167 (3):037561, 2020.
- [58] Jiwen Liu and Erik Luijten. Generalized geometric cluster algorithm for fluid simulation. *Physical Review E*, 71(6):066701, 2005.
- [59] AP Lyubartsev, AA Martsinovski, SV Shevkunov, and PN Vorontsov-Velyaminov. New approach to monte carlo calculation of the free energy: Method of expanded ensembles. The Journal of chemical physics, 96(3):1776–1783, 1992.
- [60] Carmel Majidi. Soft robotics: a perspective–current trends and prospects for the future. Soft Robotics, 1(1):5–11, 2014.
- [61] Enzo Marinari and Giorgio Parisi. Simulated tempering: a new monte carlo scheme. EPL (Europhysics Letters), 19(6):451, 1992.
- [62] Nicholas Metropolis, Arianna W Rosenbluth, Marshall N Rosenbluth, Augusta H Teller, and Edward Teller. Equation of state calculations by fast computing machines. *The journal of chemical physics*, 21 (6):1087–1092, 1953.
- [63] Mihaly Mezei. Adaptive umbrella sampling: Self-consistent determination of the non-boltzmann bias. Journal of Computational Physics, 68(1):237–248, 1987.
- [64] Devesh Mistry, Nicholas A Traugutt, Brett Sanborn, Ross H Volpe, Lillian Chatham, Risheng Zhou, Bo Song, Kai Yu, Kevin Long, and Christopher M Yakacki. Soft elasticity optimises dissipation in 3d-printed liquid crystal elastomers, 2021.

- [65] Kosar Mozaffari, Liping Liu, and Pradeep Sharma. Theory of soft solid electrolytes: Overall properties of composite electrolytes, effect of deformation and microstructural design for enhanced ionic conductivity. *Journal of the Mechanics and Physics of Solids*, page 104621, 2021.
- [66] Soumya Mukherjee, Hossein Pourmatin, Yang Wang, Timothy Breitzman, and Kaushik Dayal. Symmetry-adapted tight-binding electronic structure analysis of carbon nanotubes with defects, kinks, twist, and stretch. *Mathematics and Mechanics of Solids*, 26(5):667–682, 2021.
- [67] Ailish O'Halloran, Fergal O'malley, and Peter McHugh. A review on dielectric elastomer actuators, technology, applications, and challenges. *Journal of Applied Physics*, 104(7):9, 2008.
- [68] Paul Plucinsky, Benjamin A Kowalski, Timothy J White, and Kaushik Bhattacharya. Patterning nonisometric origami in nematic elastomer sheets. *Soft matter*, 14(16):3127–3134, 2018.
- [69] Amir Hossein Rahmati, Shengyou Yang, Siegfried Bauer, and Pradeep Sharma. Nonlinear bending deformation of soft electrets and prospects for engineering flexoelectricity and transverse (d 31) piezo-electricity. *Soft Matter*, 15(1):127–148, 2019.
- [70] Št ěpán Růžička and Michael P. Allen. Collective translational and rotational monte carlo cluster move for general pairwise interaction. *Phys. Rev. E*, 90:033302, Sep 2014. doi: 10.1103/PhysRevE.90.033302. URL https://link.aps.org/doi/10.1103/PhysRevE.90.033302.
- [71] Gareth O Roberts and Jeffrey S Rosenthal. Optimal scaling for various metropolis-hastings algorithms. Statistical science, 16(4):351–367, 2001.
- [72] Marshall N Rosenbluth and Arianna W Rosenbluth. Monte carlo calculation of the average extension of molecular chains. *The Journal of Chemical Physics*, 23(2):356–359, 1955.
- [73] James Sethna. Statistical mechanics: entropy, order parameters, and complexity, volume 14. Oxford University Press, USA, 2021.
- [74] Chris Sherlock and Gareth Roberts. Optimal scaling of the random walk metropolis on elliptically symmetric unimodal targets. *Bernoulli*, 15(3):774–798, 2009.
- [75] Michael D Shields. Adaptive monte carlo analysis for strongly nonlinear stochastic systems. Reliability Engineering & System Safety, 175:207–224, 2018.
- [76] Michael D Shields, Kirubel Teferra, Adam Hapij, and Raymond P Daddazio. Refined stratified sampling for efficient monte carlo based uncertainty quantification. *Reliability Engineering & System Safety*, 142: 310–325, 2015.
- [77] Ralph C Smith. Uncertainty quantification: theory, implementation, and applications, volume 12. Siam, 2013.
- [78] Walter H Stockmayer. Dielectric dispersion in solutions of flexible polymers. Pure and Applied Chemistry, 15(3-4):539–554, 1967.
- [79] X Sun, T Kirchdoerfer, and M Ortiz. Rigorous uncertainty quantification and design with uncertain material models. *International Journal of Impact Engineering*, 136:103418, 2020.
- [80] Robert H Swendsen and Jian-Sheng Wang. Nonuniversal critical dynamics in monte carlo simulations. *Physical review letters*, 58(2):86, 1987.
- [81] Michael Tinkham. Group theory and quantum mechanics. Courier Corporation, 2003.
- [82] Glenn M Torrie and John P Valleau. Nonphysical sampling distributions in monte carlo free-energy estimation: Umbrella sampling. *Journal of Computational Physics*, 23(2):187–199, 1977.
- [83] GM Torrie and JP Valleau. Monte carlo study of a phase-separating liquid mixture by umbrella sampling. *The Journal of chemical physics*, 66(4):1402–1408, 1977.

- [84] J. Towns, T. Cockerill, M. Dahan, I. Foster, K. Gaither, A. Grimshaw, V. Hazlewood, S. Lathrop, D. Lifka, G. D. Peterson, R. Roskies, J. Scott, and N. Wilkins-Diehr. XSEDE: Accelerating scientific discovery. *Computing in Science & Engineering*, 16(05):62–74, sep 2014. ISSN 1558-366X. doi: 10. 1109/MCSE.2014.80.
- [85] Nicholas A Traugutt, Devesh Mistry, Chaoqian Luo, Kai Yu, Qi Ge, and Christopher M Yakacki. Liquid-crystal-elastomer-based dissipative structures by digital light processing 3d printing. Advanced Materials, 32(28):2000797, 2020.
- [86] L R G Treloar. The physics of rubber elasticity. Oxford University Press, 1975.
- [87] Mark Tuckerman. Statistical mechanics: theory and molecular simulation. Oxford university press, 2010.
- [88] Paul Van Dooren and Luc de Ridder. An adaptive algorithm for numerical integration over an n-dimensional cube. *Journal of Computational and Applied Mathematics*, 2(3):207–217, 1976.
- [89] Hermann Weyl. The theory of groups and quantum mechanics. Courier Corporation, 1950.
- [90] Ulli Wolff. Collective monte carlo updating for spin systems. Physical Review Letters, 62(4):361, 1989.
- [91] Ulli Wolff. Critical slowing down. Nuclear Physics B-Proceedings Supplements, 17:93–102, 1990.
- [92] D-B Zhang, Richard D James, and T Dumitrică. Electromechanical characterization of carbon nanotubes in torsion via symmetry adapted tight-binding objective molecular dynamics. *Physical Review B*, 80(11):115418, 2009.
- [93] Jiaxin Zhang, Stephanie TerMaath, and Michael D Shields. Imprecise global sensitivity analysis using bayesian multimodel inference and importance sampling. *Mechanical Systems and Signal Processing*, 148:107162, 2021.
- [94] Ruike Zhao, Yoonho Kim, Shawn A Chester, Pradeep Sharma, and Xuanhe Zhao. Mechanics of hard-magnetic soft materials. *Journal of the Mechanics and Physics of Solids*, 124:244–263, 2019.
- [95] Yinhao Zhu and Nicholas Zabaras. Bayesian deep convolutional encoder–decoder networks for surrogate modeling and uncertainty quantification. *Journal of Computational Physics*, 366:415–447, 2018.